Carbonate system properties and anthropogenic carbon inventory in the Algerian Basin during SOMBA cruise (2014): Acidification estimate

Mehdia Asma Keraghel, Ferial Louanchi, Mohamed Zerrouki, Malik Aït Kaci, Nadira Aït-Ameur, Matthieu Labaste, Hervé Le Goff, Vincent Taillandier, Romaissa Harid, Laurent Mortier

Marine Chemistry
April 2021, Volume 221, Pages 103783 (16p.)
https://doi.org/10.1016/j.marchem.2020.103783
https://archimer.ifremer.fr/doc/00615/72729/

Carbonate system properties and anthropogenic carbon inventory in the Algerian Basin during SOMBA cruise (2014): Acidification estimate

Keraghel Mehdia Asma [1, *], Louanchi Ferial [1], Zerrouki Mohamed [1], Kaci Malik Ait [1], Aït-Ameur Nadira [1], Labaste Matthieu [2], Legoff Hervé [2], Taillandier Vincent [3], Harid Romaissa [4], Mortier Laurent [2]

[1] CVRM: Laboratoire de Conservation et de Valorisation des Ressources Marines, Ecole Nationale Supérieure des Sciences de la Mer et de l'Aménagement du Littoral (ENSSMAL), Station de recherche de Sidi Fredj, Algeria
[2] LOCEAN: Laboratoire d'Océanographie et du Climat: Expérimentations et Approches Numériques, Unité Mixte de Recherche 7159 CNRS/IRD/Université Pierre et Marie Curie/MNHN, Institut Pierre Simon Laplace, place Jussieu, 75252 Paris, France
[3] LOV: CNRS, Laboratoire d'Océanographie de Villefranche, Sorbonne Universités, Villefranche-sur-Mer, France
[4] ECOSYSMarL: Laboratoire des Écosystèmes Marins et Littoraux, ENSSMAL, Station de recherche de Sidi Fredj, Algeria

* Corresponding author : Mehdia Asma Keraghel, email address : ma.keraghel@enssmal.dz

f.louanchi@enssmal.dz ; m.zerrouki@enssmal.dz ; m.ait-kaci@enssmal.dz ; matthieu.labaste@locean-ipsl.upmc.fr ; herve.legoff@locean-ipsl.upmc.fr ; taillandier@obs-vlfr.fr ; r.harid@enssmal.dz ; mortier@locean-ipsl.upmc.fr

Abstract :

Recent studies have provided a better understanding of carbonate system parameters and their spatial and temporal variability in several areas of the Mediterranean Sea. This study uses a new dataset that covered the entire Algerian Basin during the summer of 2014 (SOMBA cruise) to describe the distribution of carbonate system parameters. The findings show that almost the entire basin was a source of CO2 to the atmosphere during the studied period. Besides the well-known TrOCA (Tracer combining Oxygen, Carbon and total Alkalinity) approach, the study proposes new parametrization for the standard back calculation method to assess the anthropogenic carbon concentration. The results of both approaches yield similar distributions and concentration ranges (81 ± 4.3 and 69 ± 5.2 µmol/kg, respectively). This study assesses the errors for both approaches and emphasizes the importance of mesoscale and submesoscale structures on anthropogenic carbon sequestration and the distribution of carbonate parameters in the Algerian Basin. It shows that these features enhance basin ventilation and acidification. The first inventory of the anthropogenic carbon trapped by the Algerian Basin is estimated at 0.44–0.53 ± 0.06 Pg C, based on the new dataset.

Highlights

► The first high resolution spatial coverage of the Algerian Basin allowed a detailed study of the carbonate parameters. ► A refitted back-calculation method is applied to estimate anthropogenic carbon concentrations. ► Highlighting the role of the submesoscale processes in the increase of anthropogenic carbon sequestration. ► The estimated acidification of the Algerian Basin, from the preindustrial era to 2014, range between −0.19 and −0.1 pH unit. ► The first estimate of the anthropogenic carbon inventory trapped by the Algerian Basin is at 0.44–0.53 ± 0.06 Pg C.

Keywords : Algerian Basin, Carbonate system, Anthropogenic carbon inventory, Acidification, Mesoscale activity

Introduction

The Mediterranean Sea (MS) plays a relevant role in anthropogenic carbon (C^{ant}) sequestration because it is highly sensitive to global warming and climate change (Álvarez et al., 2014; Touratier et al., 2012). The MS has built up larger C^{ant} inventories throughout its water column than the global ocean (Lee et al., 2011; Schneider et al., 2010). This is caused by its elevated Total Alkalinities (TA), a Revelle Factor of ~9 in surface waters, and its active water circulation. Moreover, many authors showed that the MS is a source of CO_2 to the Atlantic Ocean (e.g., Aït-Ameur and Goyet, 2006; Huertas et al., 2009), whence the growing interest in assessing the sequestered C^{ant} into this marginal sea during the last few decades (Malanotte-Rizzoli et al., 2014).

The scientific community took an interest in the amount of sequestered C^{ant} in the MS in the early 2000s. The temporal evolution of C^{ant} concentrations, from the mid-1990 to the mid-2000, was studied at the DYFAMED (Dynamique des Flux Atmosphériques en Mediterranée) site using the TrOCA approach (Touratier and Goyet, 2009). This work was later expanded throughout the MS by Touratier and Goyet (2011) using the METEOR M51/2 dataset (2001). Schneider et al. (2010) applied an indirect method to the same dataset to estimate the amount of C^{ant} trapped in the eastern basin of the MS (TTD Method: Transient Time Distribution). Aït-Ameur and Goyet (2006), Huertas et al. (2009), and Rivaro et al. (2010) also applied the TrOCA approach to estimate the C^{ant} concentrations in the Strait of Gibraltar and other locations around the MS. In 2012, Touratier et al. (2012) re-estimated the C^{ant} concentrations based on the BOUM dataset (Biogéochimie de l'Oligotrophie à l'Ultra-oligotrophie de la Méditerranée) collected in 2008. This study compared two direct approaches, the TrOCA and the MIX—optimum multiparameter MIXing analysis—to estimate the C^{ant} accumulation at about 0.8–1.2 $\mu mol.kg^{-1}.yr^{-1}$. In 2013, the MedSea dataset (Mediterranean Sea Acidification

in A Changing Climate) allowed Hassoun et al. (2015a) to record C^{ant} concentrations as high as 102 µmol/kg through the TrOCA approach. Such high values indicate the acidification of the MS being between -0.15 and -0.05 pH units (Hassoun et al., 2015a; Touratier and Goyet, 2011). This places the MS at the top of the most acidified marine ecosystems (Touratier et al., 2012). The C^{ant} concentrations in the MS were also estimated using either a high-resolution regional model (Palmiéri et al., 2015) or the temporal variations of the stable carbon isotope ratio of dissolved inorganic carbon in the Levantine Basin (Sisma-Ventura et al., 2016).

The aforementioned studies highlighted the important role of the western MS in trapping C^{ant}, particularly, in the Algerian Basin (AB). They promoted a better understanding of the basin's role in the regional carbon cycle and C^{ant} sequestration. The AB's complex mesoscale features (the Algerian Current, anticyclonic eddies, cyclonic gyres) are essential for spreading the Modified Atlantic Waters (MAW) in the MS and modulating the trophic regime of the AB. Nevertheless, the effects of these physical structures on the carbonate system and its anthropogenic fraction have not been studied thoroughly (e.g., Moutin and Prieur, 2012). This region has seldom been investigated by oceanographic cruises over the past few decades (e.g., the METEOR cruises in October 2001 and April 2011, the BOUM in June 2008, and the MedSea in May 2013). Additionally, these cruises have not covered important areas of the AB.

This work benefits from a new dataset collected in the summer of 2014 that completely covers the AB. The SOMBA cruise (Système d'Observations à la mer dans le Bassin Algérien) was conducted in the context of MERMEX (Marine Ecosystems' Response in the Mediterranean Experiment Program) that aims at studying the influence of global warming and anthropogenic activities on the marine ecosystems of the MS (Durrieu de Madron et al., 2011). First, we addressed the spatial distribution of carbonate system parameters in the AB by focusing on the east-west and north-south gradients. Second, the C^{ant} concentration was

estimated using the TrOCA approach (Touratier et al., 2007) in addition to a refitted Chen and Millero (1979) method that was parametrized for preindustrial conditions using knowledge on the MS carbonate system acquired over the last two decades. Finally, the C^{ant} concentrations obtained using the two methods were discussed, emphasizing the role of mesoscale activity on the distribution of this parameter. A first estimate of the amount of C^{ant} sequestered by the AB from the preindustrial period to the summer of 2014 was derived from this new dataset.

1 Material and Methods

1.1 SOMBA dataset

The SOMBA cruise, dedicated to studying the AB, was conducted between August 14th and September 10th, 2014 on the French R/V "Téthys II" (Mortier et al., 2014). This French-Algerian cruise had four legs, including sampling at 70 hydrological stations along 7 sections (Fig. 1). At each station, an underwater sampling system was lowered from the surface to the bottom. The system included a SeaBird SBE911+ CTD (Conductivity-Temperature-Depth) unit and a carousel of 11 Niskin bottles (12 L each). The temperature and practical salinity were measured with a precision of ±0.002 °C and ±0.003, respectively. The data were pretreated through manual check outs and spike removal. The instrumentation errors were corrected by applying the SBE Data Processing software. The sensors' drift was corrected based on the manufacturer's recommendations, in addition to salinity measurements of discrete samples, taken directly from the Niskin bottles, using an autosalinometer. The CTD was also interfaced with a dissolved oxygen sensor (SBE43). Each station was sampled over eleven depth levels. Discrete samples were collected for dissolved oxygen (12 stations), Dissolved Inorganic Carbon/Total Alkalinity (DIC/TA) (22 stations) and nutrients (70 stations).

Dissolved oxygen sensor responses were calibrated using daily oxygen measurements performed by Winkler potentiometric titrations, based on Longdon (2010)'s modified method. The sensor's calibration coefficients were statistically adjusted by using multiple Winkler water samples and sensor voltages over a wide range of oxygen calculations (SBE, 2010). Thirty-two duplicates were sampled at different depths with an estimated precision of 1.6 µmol/kg. Quality control checks were performed for all the parameters, based on the recommendations of the Global Ocean Ship-based Hydrographic Investigations Program (Go-SHIP) (Swift, 2010). Subsequently, the data were flagged using World Ocean Circulation Experiment (WOCE) standards. Only data deemed "good" were selected for this study.

1.2 Geochemical parameters measurements

Carbonate system parameters were sampled in 500 ml borosilicate glass vials (222 samples) and poisoned with 100 µl of a saturated mercuric chloride solution ($HgCl_2$), based on Dickson et al. (2007)'s recommendations. Subsequently, the samples were analyzed for DIC and TA at the SNAPO-CO_2 Laboratory (Service National d'Analyses des Paramètres Océaniques du CO_2, France) through closed-cell potentiometric titration, based on the procedure described by Edmond (1970). The non-linear least squares procedure described in DOE (1994) was used to determine equivalent points. Thirteen duplicates were homogeneously sampled over the cruise's time and space scales. Their repeatability was expressed using the short-term standard deviation—2 µmol/kg and 3.3 µmol/kg for TA and DIC, respectively. The absolute differences (R) of the duplicate measurements did not exceed the Upper Control Limit described by Dickson et al. (2007) —UCL = 3.267×R: 6.5 µmol/kg and 10.7 µmol/kg for TA and DIC, respectively. Temporal drifts of the concentration of the diluted hydrochloric acid solution were corrected using Dickson Certified Reference Materials (CRM) provided by the University of California- San Diego (batch 139: TA=2250.8±0.6 µmol/kg, DIC=2023.2±0.7

µmol/kg). Nutrient concentrations were determined by an automatic colorimetric procedure with a Technicon Auto Analyzer (Tréguer and LeCorre, 1975) at the MIO Laboratory (Mediterranean Institute of Oceanography- France). The precision of the nitrite, nitrate, soluble reactive phosphate, and silicic acid measurements was 2 %, 3–5 %, 3–5 %, and 5 %, respectively while the detection limits were 0.03 µM, 0.05 µM, 0.02 µM, and 0.05 µM, respectively.

1.3 Carbonate system parameter calculations

Carbonate system properties were sampled at 22 stations of the SOMBA cruise. We computed multiparametric linear regressions for TA and DIC, versus potential temperature (θ), practical salinity (S_P), and Apparent Oxygen Utilization (AOU) to extrapolate discrete TA and DIC measurements over the entire basin. Researchers have already reported a linear relationship between the TA and S_p in the MS (Copin-Montégut and Bégovic, 2002; Hassoun et al., 2015b). Nevertheless, this correlation depends on the region of the MS (e.g., Cossarini et al., 2015) and seems stronger in the AB, characterized by fewer sources of TA variability than the eastern MS (the riverine and the Dardanelle inputs). Lee et al. (2006) also showed that temperature can partly explain TA variability.

DIC variability depends on both physical and biological processes (e.g., Goyet and Davis, 1997) and was expressed against θ, S_P, and AOU. Several equations were tested for TA and DIC interpolations using the SOMBA cruise data, either by accounting for the entire water column or by dividing the dataset into three layers (surface, intermediate, and deep waters). Regressions for the eastern and western gyres of the AB were also tested based on Testor et al. (2005)'s findings. Additionally, we evaluated previously published equations for the AB (Gemayel et al., 2015; Hassoun et al., 2015b; Touratier and Goyet, 2009; Touratier and Goyet, 2011). The Root Mean Square Deviation (RMSD) always exceeded 20 µmol/kg for

the latter equations. The most appropriate equations for the intermediate and deep waters were found to be (±RMSD):

$$TA = 131.005\, S_p - 9.118\, \theta - 2329.812 \text{ (±4.6 µmol/kg)} \quad (1)$$

$$DIC = 64.812\, S_p - 5.384\, \theta + 0.483\, AOU - 120.117 \text{ (±8.2 µmol/kg)} \quad (2)$$

These equations offer an acceptable coefficient of determination (0.62 and 0.98 for TA and DIC, respectively), a mean residual value of 0, and the lowest standard deviation of the residuals (SD_R) and RMSD (4.6 µmol/kg and 8.2 µmol/kg for TA and DIC, respectively) for intermediate and deep layers. This is equivalent to an error of 0.13% and 0.36% for averaged TA and DIC concentrations, respectively. It is within twice the measurement precision (Fig. 2).

TA and DIC data were normalized to the practical salinity based on the procedure developed by Friis et al. (2003). The following equations were applied:

$$NTA = \frac{TA - TA^{S=0}}{S_p} \times S^{ref} + TA^{S=0} \text{ with } TA^{S=0} = -998\ \mu mol/kg \quad (3)$$

$$NDIC = \frac{DIC - DIC^{S=0}}{S_p} \times S^{ref} + DIC^{S=0} \text{ with } DIC^{S=0} = -2215\ \mu mol/kg \quad (4)$$

where $TA^{S=0}$ and $DIC^{S=0}$ are the non-zero freshwater endmembers and S^{ref} is the reference salinity (38 for the MS).

The pH on the total proton concentration scale (pH_T) and the partial pressure of CO_2 (pCO_2^{sw}) were calculated using the CO2SYS macro, version 2.1 (Pierrot et al., 2006). The parameters were set to follow the recommendations of Álvarez et al. (2014): equilibrium constants K_1 and K_2 from Mehrbach et al. (1973), as refitted by Dickson and Millero (1987); the sulphate dissociation constant from Dickson (1990); the total boron-salinity relationship from Uppström (1974). The SOMBA silicate and soluble reactive phosphate concentrations with

their relevant constants were also used. The air-sea gradient of pCO_2 (ΔpCO_2), the difference between the oceanic and atmospheric pCO_2 (pCO_2^{sw} and pCO_2^{air}, respectively), was calculated using the following equations:

$$\Delta pCO_2 = pCO_2^{sw} - pCO_2^{air} \quad (5)$$

$$pCO_2^{air} = xCO_2 \times (patm - pH_2O) \quad (6)$$

where xCO_2 is the Atmospheric Carbon Dioxide Dry Air Mole Fraction retrieved from the World Data Centre for Greenhouse Gases ("WDCGG," 2018). Six stations located around the AB were selected to compute the mean xCO_2 for the two periods between 17–31 August and 01–08 September (390±2.8 ppm and 393±2.4 ppm, respectively) (Table 1). *p*atm is the atmospheric pressure, obtained from the NCEP/DOE AMIP-II Daily reanalysis (Reanalysis 2) averages gridded at a 2.5º resolution. The data for this analysis were provided by the NOAA/OAR/ESRL PSD (Kanamitsu et al., 2002). pH_2O is the water vapor pressure calculated according to Weiss and Price (1980)'s equation, assuming that the air above the air-sea interface is water saturated.

1.4 Anthropogenic carbon inventory

The AB was divided into a grid of eleven boxes of 2° longitude by 2° latitude each to compute the inventory of its sequestered C^{ant}. A vertical profile of C^{ant} concentrations for each box was calculated by averaging the data from layers of varying thicknesses, ranging from 150 m to the ocean floor, following the MEDAR/MEDATLAS (Mediterranean Data Archaeology and Rescue) vertical grid standard (Equation 7). The sum of all the boxes represents the total C^{ant} inventory of the AB. The associated uncertainty was assessed by an error propagation equation.

$$C_{box-inv}^{ant}(g\ C) = \left[\sum_{i=150m}^{bottom} (C_i^{ant} \times dz_i \times \rho_i) \times 12 / (z_{bottom} - 150)\right] \times Vol_{box} \quad (7)$$

where $C^{ant}_{box-inv}$ is the anthropogenic carbon inventory for each box in grams of carbon (g C); C^{ant}_i is the computed anthropogenic carbon concentration (mol/kg); dz_i is the corresponding thickness of the layer (m); ρ_i is water density expressed in kg/m^3; 12 is the atomic mass of carbon (g/mol); Z_{bottom} is the bottom depth of the profile (m); Vol_{box} is the computed volume of the box (m^3), based on the AB bathymetry provided by the General Bathymetric Chart of the Oceans (GEBCO, 2019).

2 Results and Discussion

2.1 Anthropogenic carbon and acidification assessment

In this study, we calculated the C^{ant} concentration using two different approaches. First, the back-calculation technique proposed by Chen and Millero (1979). Second, the TrOCA method proposed by Touratier et al. (2007). The methods were selected for their simplicity, data availibility, and adaptability to the characteristics of the MS. They were not applied to the mixed surface layer (0-150 m) because of its physical and chemical variability (air-sea exchanges and biological processes).

2.1.1 The Chen and Millero (1979) approach (MCM)

The measured DIC includes a natural (preformed, preindustrial carbon, $C^{0,PI}$) and an anthropogenic fraction (C^{ant}), in addition to the *in-situ* DIC generated (or consumed) by biological processes (C^{bio}). Consequently, anthropogenic carbon concentration is calculated as:

$$C^{ant} = DIC - C^{bio} - C^{0,PI} \quad (8)$$

with: $$C^{bio} = 0.5\,\Delta TA - (C/O_2 + 0.5\,N/O_2).\Delta O_2 \quad (9)$$

$$\Delta TA = TA - TA^0 \; and \; \Delta O_2 = O_2^0 - O_2^{mes} = AOU \quad (10)$$

where TA and TA^0 correspond to the measured and preformed alkalinity, respectively. TA^0 is calculated by applying Equation 11, derived from the SOMBA surface data (0–150 m).

$$TA^0 = 93.779\ S_p - 0.57\ \theta - 1004.765\ (\pm 7.5\ \mu mol/kg) \quad (11)$$

C/O_2 and N/O_2 are the molar ratios proposed by Anderson (1995) based on the average composition of planktonic organic matter (C:N:P:-O_2=106:16:1:-150); O_2^{mes} and O_2^0 are the measured and preformed dissolved oxygen concentrations, respectively; ΔO_2 can be equated to AOU. The preformed oxygen concentration is usually assumed to be equal to the saturation value with respect to the atmosphere. At the DYFAMED site, 20 years of observational data reveal that seawater is undersaturated with respect to oxygen in winter (Copin-Montégut and Bégovic, 2002 ; Coppola et al., 2018). Therefore, in this study, the preformed oxygen is assimilated to a seawater undersaturation of 4% that corresponds to the winter mean observations in the deep-water formation area. In the western MS, this area lies in the Gulf of Lion, off the French coast. Seawater oxygen saturation is calculated using the equation of Benson and Krause (1984).

2.1.1.1 **Preformed, preindustrial carbon parametrization ($C^{0,PI}$)**

All water masses in the MS have already been contaminated by C^{ant} because of their short water renewal time. The preformed, preindustrial DIC concentration ($C^{0,PI}$) can be determined by assuming a preindustrial partial pressure of CO_2 (pCO_2) of 280 ppm and a constant preformed alkalinity (TA^0) (Equation 11). This simplified parametrization corresponds to the C* of Gruber et al. (1996). This term also accounts for the air-sea disequilibrium of CO_2 when water masses were last in contact with the atmosphere. Several studies in the deep-water formation region show that seawater is undersaturated with respect to CO_2 in winter, with a maximum undersaturation of -80 µatm and a mean value between -30 µatm to -40 µatm, depending on the investigated time-period. This result is based on the *in-situ* data at the

DYFAMED site (Copin-Montégut et al., 2004; Hood and Merlivat, 2001) and on regional model outputs (D'Ortenzio et al., 2008; Taillandier et al., 2012). Thus, computing a preindustrial, preformed DIC from a 280 ppm pCO_2 systematically underestimates the C^{ant} concentration, since it overestimates the $C^{0,PI}$. Therefore, we chose to compute $C^{0,PI}$ by considering a pCO_2 undersaturation of -30 µatm (water pCO_2=250 µatm) during winters for the preindustrial era. We will use the acronym MCM for the Modified Chen and Millero (1979) approach.

2.1.1.2 **Sensitivity tests and uncertainty estimation**

The MCM approach is based on three main assumptions: 1. biological activity remains constant over time; 2. the MS is at a steady state; 3. the air-sea winter disequilibrium in the deep-water formation area has been constant since the preindustrial period. Sensitivity tests have been performed to assess the errors in the selected parametrization used to calculate C^{ant} concentrations (systematic errors). We conducted four sets of tests:

- The preformed alkalinity was calculated using two equations: Hassoun et al. (2015b)'s equation for the Liguro-Provencal surface waters (0–25 m) derived from the MEDSEA cruise (TA^0=120.72 S_p−1282.6) and Copin-Montégut and Bégovic (2002)'s equation for surface waters at the DYFAMED site (TA^0=93.996 S_p−1038.1).
- We used another set of stoichiometric ratios (Körtzinger et al., 2001) corresponding to the revised Redfield ratios with a corrected carbon coefficient for the anthropogenic CO_2 (C:N:P:O_2=123:17.5:1:-165).
- A 2% undersaturation of seawater was tested instead of 4% for the preformed oxygen concentrations, considering that the oxygen solubility pump may enhance oxygen concentrations in cold surface waters.

- Taillandier et al. (2012) showed that the winter air-sea ΔpCO_2 is decreasing (pCO_2^{atm} is rising faster than that of the ocean). Thus, we tested an undersaturation of -20 µatm (pCO_2=260 µatm) for the preindustrial situation.

The random error associated with the estimated C^{ant} concentrations was computed through error propagation using the formula described in Gruber et al. (1996), assuming that the errors were independent of each other ($\sigma_{O_2} = 1.6$ µmol/kg, $\sigma_{O_2^0} = 4.9$ µmol/kg, $\sigma_{TA} = 2$ µmol/kg, $\sigma_{TA^0} = 7.5$µmol/kg, $\sigma_{DIC} = 3.3$ µmol/kg, $\sigma_{C^{0,PI}} = 3$ µmol/kg, $\sigma_{\frac{C}{O_2}} = 0.0816$, $\sigma_{\frac{N}{O_2}} = 0.0097$) (Table 2). The RMSD values between the selected and tested parametrizations for the four parameters are reported in Table 3.1. The total error in C^{ant} concentrations was 8.3 µmol/kg with a maximum error of about 12.6 µmol/kg (considering the values of $\sigma_{C^{0,PI}}$ and σ_{TA^0} from Table 3.1). Subsequently, the retained uncertainty is ±10 µmol/kg. This is 9.2% of the computed C^{ant} values. Table 3.2 shows that stoichiometric parametrization causes the lowest error on the calculation of C^{ant} concentrations (2.2 µmol/kg). Preformed oxygen and TA parametrizations generate an uncertainty of the same order of magnitude (3 µmol/kg), whereas the estimate of $C^{0,PI}$ introduces an error of up to 9.4 µmol/kg. Nevertheless, the sensitivity tests' results illustrate that systematic errors in estimating C^{ant} concentrations through the MCM approach are acceptable and lie within the estimated random error of 10 µmol/kg.

2.1.2 The TrOCA approach

The TrOCA is a semi-conservative-tracer model developed by Touratier and Goyet (2004). The model was later improved to better estimate the preindustrial term $TrOCA^0$ (Touratier et al., 2007), and used by the authors, in combination with three tracers ($\Delta^{14}C$, CFC-11, and ^3H), to identify old oceanic water masses that are unaffected by the anthropogenic carbon invasion

in the global ocean. The $TrOCA^0$ was computed as a function of two measurable parameters (TA and θ). This approach assumes constant stoichiometric ratios, TA, and oxygen concentrations (O_2). The anthropogenic carbon concentration is calculated using the following equation:

$$C_{Ant}^{TrOCA} = \frac{O_2 + 1{,}279\left[DIC - \frac{1}{2}TA\right] - exp\left(7.511 - \left(1.087 \times 10^{-2}\right)\theta - \frac{7.81 \times 10^5}{TA^2}\right)}{1.279} \quad (12)$$

The estimated uncertainty for this method is ±9.8 µmol/kg (8.5% of the C^{ant} maximum value), using the error propagation equation described by Touratier et al. (2007).

2.1.3 Acidification assessment

The change in the AB's pH from the preindustrial period to 2014 (ΔpH) was calculated using the following equation:

$$\Delta pH = pH_{2014} - pH_{preind} \quad (13)$$

where pH_{2014} is the computed total pH described in section (1.3); pH_{preind} is the pH_T of preindustrial era calculated using the preindustrial TA (assuming that TA remains constant over time) and the preindustrial DIC (DIC_{preind}). The latter was estimated by subtracting the computed anthropogenic fraction from the measured DIC:

$$DIC_{preind} = DIC - C^{ant} \quad (14)$$

2.2 The distribution of carbonate system properties

2.2.1 Physical settings

A hydrological study was conducted before studying the distribution of the carbonate system parameters. It used θ/S_p diagrams and the vertical distribution of practical salinity (Fig. 3). Consequently, the basin was separated into three layers. First, the surface layer (0–150 m),

characterized by Atlantic Waters (AW) that penetrate the AB from the Almeria-Oran front, with an Atlantic salinity signature of 36.7. Fig. 1 reveals active mesoscale activity during the SOMBA cruise, characterized by a significant anticyclonic eddy with a Sea Level Anomaly (SLA) of about 0.35 m centered in the eastern part of the basin at 38.2 °N/5.8 °E. The Algerian Current shows these baroclinic instabilities throughout its eastward progression (Millot and Taupier-Letage, 2005).

Second, the intermediate layer (150–800 m), mainly marked by the Levantine Intermediate Waters (LIWs) that penetrate the AB through the Sardinian Channel, with temperatures between 13.6 °C and 14.17 °C and salinities between 38.5 and 38.75. The LIWs are characterized by their minimum oxygen concentrations (165–170 µmol/kg) and high salinities. They flow northward along the western Sardinian coasts to begin their cyclonic path in the western MS, as described in Millot and Taupier Letage (2005). Fig. 3b and Fig. 3d illustrate the separation between the intermediate waters of the eastern (~4 °E–10 °E) and the western (~1 °W–4 °E) parts of the basin, a separation that seems to be related to the AB's two cyclonic gyres mentioned by Testor et al. (2005). The eastern part of the basin is characterized by a thick layer of younger, warmer, and saltier waters, while the western part is characterized by older LIWs that have been mixed with surrounding waters (Hainbucher et al., 2014). The entrainment of less salty, sub-surface waters and portions of LIWs being torn apart at the center of the basin substantiate the influence of the anticyclonic eddy observed at 6 °E, an observation that corroborates Moutin and Prieur (2012) and Millot and Taupier-Letage (2005)'s findings.

Third, the deep layer (800 m–bottom) is represented by homogeneous Western Mediterranean Deep Waters (WMDWs) with a salinity of 38.48 and a temperature of 12.9 °C, in agreement with earlier observations (e.g., Béthoux et al., 2002; Schroeder et al., 2010). The bottom of the basin is almost entirely covered by more oxygenated, newly formed WMDWs (WMDWn,

Fig. 3c), characterized by slightly higher salinities and temperatures (38.49 and 12.91 °C, respectively) than the usual WMDWs. These waters are probably the result of the Western Mediterranean Transient (WMT) described by Schroeder et al. (2008).

2.2.2 Surface waters (0–150 m)

Surface TA and DIC concentrations range between 2400 and 2600 µmol/kg and between 2075 and 2334 µmol/kg, respectively. Their mean values are 2517±46 µmol/kg and 2227±55 µmol/kg, respectively (Fig. 4). According to Gemayel et al. (2015), summer conditions favor high TA and DIC concentrations in the AB due to the coastal upwellings driven by summer wind regimes (Bakun and Agostini, 2001). Surface pH_T values range between 7.97 and 8.17 with a mean value of 8.07±0.03, whereas pCO_2 concentrations vary between 294 µatm and 502 µatm with a mean value of 400±35 µatm, as observed by Copin-Montégut and Bégovic (2002) and Rivaro et al. (2010).

Surface AW flowing eastward from Gibraltar in the southern part of the AB have a low TA and DIC signature (Fig. 5a and 5c). The waters' increasing salinity causes the increasing eastward and northward gradients of the inflowing waters (Fig. 5h) that gain Mediterranean characteristics along their cyclonic path (S_p=36.7 to 38.5). According to Millero et al. (1998), salinity contributes to 80% of TA variability in surface waters in major ocean basins (Atlantic, Pacific, and Indian Oceans). Cossarini et al. (2015) observed similar distributions of TA in the MS and attributed the north-south gradient to terrestrial inputs. Several researchers noticed similar trends for the DIC distribution using different approaches (e.g., Álvarez et al., 2014; Gemayel et al., 2015; Hassoun et al., 2015b; Schneider et al., 2010). Although our data clearly show that salinity controls the surface TA and DIC variability, the normalized values provide insights about the biogeochemical drivers for these distributions. For instance, the western part of the basin hosts the maximum normalized alkalinities (Fig. 5b), corresponding with

oxygen oversaturation (Fig. 5g) and CO_2 undersaturation of the seawater (Fig. 5f). The latter may imply that the slight increase in TA is associated with photosynthetic activity. Moreover, the NDIC distribution presents a decreasing northward gradient. This suggests that the Algerian Current, and thereby the Atlantic waters, are a source of DIC to the MS (Huertas et al., 2009).

Inflowing AW have high pH values (Fig. 5e), likely associated with CO_2 consumption through photosynthesis. This makes the southwestern part of the AB a CO_2 sink in late summer. The surface dissolved oxygen and pCO_2 values are strongly correlated (R=0.93), as also reported by Rivaro et al. (2010). Meanwhile, the more oligotrophic MAWs exhibit lower pH values and are a source of CO_2 to the atmosphere over most of the basin (ΔpCO_2=+75±29 µatm) (Fig. 5f). This is probably caused by the high surface temperatures (20–27 °C) in summer (high correlation between pCO_2 and surface temperatures—R=0.84), in agreement with the findings of Bégovic and Copin-Montégut (2002), D'Ortenzio et al. (2008), and Louanchi et al. (2009). The increasing eastward pCO_2 gradient was also observed by several researchers in response to the increased TA and DIC concentrations (e.g., D'Ortenzio et al., 2008; Gemayel et al., 2015; Rivaro et al., 2010; Taillandier et al., 2012). These authors mainly associate pCO_2 variability with physical processes (water mixing, air-sea exchange, salinity and temperature) and, to a lesser extent, primary production.

2.2.3 Intermediate and deep waters (150 m–bottom)

The TA and DIC concentrations increase with depth and range from 2484 to 2620 µmol/kg and from 2229 to 2357 µmol/kg, respectively (Fig. 4), as corroborated by many studies (Álvarez et al., 2014; Hassoun et al., 2015b; Touratier et al., 2012). The spatial distribution of TA and DIC is related to water mass distributions: maximum TA and DIC concentrations are observed in the older and saltier core of the LIWs at around 450 m (Fig. 6a and Fig. 6c); the

WMDWs exhibit lower TA and DIC concentrations because they are younger and better oxygenated by deep-water formation processes. The NTA and NDIC distributions do not provide more insights about their variability, except a few anomalies around 6 °E that may be associated with organic matter remineralization in a mesoscale structure (Fig. 6b and 6d). Such anomalies (higher DIC and lower TA concentrations) were also reported during the BOUM cruise by Touratier et al. (2012). According to Hassoun et al. (2015b), the MS' active overturning circulation enriches deep waters with labile carbon that promotes significant increases in DIC concentration through remineralization. Moreover, convection and advection of dense waters is a more important sink for organic carbon than the sedimentation of particulate matter from the upper layers of the MS (La Ferla et al., 2003).

Fig. 7 shows the latitudinal and longitudinal mean concentrations of DIC and TA for non-normalized and normalized data. The results are presented for three depth layers (surface, intermediate, and deep). The surface longitudinal and latitudinal distributions illustrate important fluctuations (through the error bars) and confirm previous observations—decreasing gradients eastward for both salinity-normalized parameters (NTA, NDIC) (Fig. 7c and Fig. 7d) and a distinct northward decreasing gradient for the NDIC (Fig. 7h). These gradients persist for NDIC in the intermediate layer due to higher organic matter remineralization in older waters. However, the NTA distribution does not show a significant gradient because biological processes do not impact it much. The non-normalized TA and DIC distributions display an eastward gradient in the intermediate and deep waters. This finding contrasts with Lovato and Vichi (2015) and Cossarini et al. (2015), who reported that the eastward gradient of TA and DIC disappears at a depth of 250 m. Deep waters present only small variations with eastward trends within the uncertainty range for both the normalized and non-normalized data.

2.3 Anthropogenic carbon

2.3.1 Anthropogenic carbon distribution

Fig. 8 shows the C^{ant} concentration estimates from the two approaches. The concentrations are different but display similar spatial distributions. Generally, they reach the highest values in the upper layer (150–250 m) that is in direct contact with the enriched surface waters (TrOCA:70–115 µmol/kg; MCM: 59–109 µmol/kg). The inflow of old LIWs to the western MS basin in the intermediate layer (400–1000 m) is characterized by the lowest C^{ant} concentrations (TrOCA: 61–99 µmol/kg; MCM: 50–91 µmol/kg). These concentrations increase in deep waters that are continuously renewed by deep-water formation processes in the Gulf of Lion (TrOCA: 69–100 µmol/kg; MCM: 56–83 µmol/kg). Recently, Touratier et al. (2016) provided additional insights about the important role of deep-water formation (convection, cascading) on C^{ant} sequestration in the western MS.

The observed values, similar to those of Hassoun et al. (2015a)'s for the MS in 2013, are higher than earlier estimates (Touratier and Goyet, 2011; Touratier et al., 2012). This increasing trend can be explained by the increasing concentrations of atmospheric and surface water CO_2, which were confirmed by Marcellin Yao et al. (2016). The intense deep-water convection and cascading recorded in the western MS between 2005 and 2013 (Houpert, 2013; Puig et al., 2013; Schroeder et al., 2008) could have influenced C^{ant} concentrations in the AB during the SOMBA cruise. The inflowing Atlantic waters may also be a potential source of C^{ant} in the AB (Huertas et al., 2009).

The vertical distribution of AOU (Fig. 8c) shows that the mesoscale structures observed during the SOMBA cruise are characterized by less oxygenated waters and lower C^{ant} concentrations. This is probably caused by anticyclonic eddies that trap older intermediate waters and entrain them to depth. According to Moutin and Prieur (2012), these structures

function as closed systems and their vortex barrier prevents large-scale mixing, water advection, and renewal through deep-water formation. Nevertheless, an anomaly with high C^{ant} concentrations can be observed near the anticyclonic eddy at 6 °E. It was associated with high DIC and low TA concentrations, while dissolved oxygen concentrations were not significantly anomalous. This could be explained by the entrainment of newly formed waters from their formation area (Gulf of Lion) to the AB by anticyclonic Submesoscale Coherent Vortices (SCV). In fact, Testor and Gascard (2003) observed such physical structures in the AB and demonstrated that SCVs can advect newly formed WMDW over long distances from their source. Their rotation generates transport barriers that drastically reduce lateral exchange between the core and surrounding waters. This improves their efficiency at transporting physical and biogeochemical tracers from their origin (Bosse et al., 2016). These SCVs can also strongly interact with eddies (Testor and Gascard, 2003), which could be the case for the eddy observed at 6 °E during the SOMBA cruise. The newly formed and advected waters may be enriched with labile organic carbon that consumes the replenished oxygen through remineralization during their transport. This may explain the lack of a positive dissolved oxygen anomaly. Kessouri et al. (2018) showed that the total organic carbon export to deep waters in the MS' deep-convection area is eight times higher than in the stratified area.

2.3.2 Comparing the selected approaches

The MCM method yields lower C^{ant} concentrations than the TrOCA approach, but within the range of the C^{ant} uncertainty (~ 10 µmol/kg) (Table 4). In the last two decades, the TrOCA approach has proven its efficiency and has been accepted as a reliable method for C^{ant} assessment in the global ocean (Álvarez et al., 2009; Lo Monaco et al., 2005; Vázquez-Rodríguez et al., 2009) and in the MS (Rivaro et al., 2010; Touratier et al., 2016; Touratier and Goyet, 2009). Nevertheless, some authors suggest that the TrOCA approach might

overestimate C^{ant} concentrations (Flecha et al., 2012; Huertas et al., 2009). Recently, Sabine and Tanhua (2010) reviewed the C^{ant} assessment methods and questioned the $TrOCA^0$ parametrization and its definition of the preformed values. One may ask: Is the global ocean-based parametrization of the $TrOCA^0$ applicable to the MS? Do the MS waters (high salinity and alkalinity concentrations) have the same preindustrial properties as the global ocean? Yool et al. (2010) showed that the TrOCA approach leads to a factor of two error on the global inventory when including marginal seas. Nevertheless, our results show a strong correlation between the TrOCA and the MCM approaches, if the later used Mediterranean parametrizations. This suggests that, based on our results and sensitivity tests, the TrOCA approach is a good proxy for C^{ant} assessment in the Western MS. The first source of error in the C^{ant} estimates using the MCM approach is the assessment of CO_2 air-sea disequilibrium. This could lead to a 10 µmol/kg uncertainty (Table 3.2), in agreement with Friis (2006)'s results. In this context, winter undersaturation of the western MS probably increased with the increase in atmospheric pCO_2 (Taillandier et al., 2012). Nevertheless, a recent study by Touratier et al. (2016) shows that during the deep-water convection event in the winter of 2011, the sea-surface waters acted as a source of CO_2 to the atmosphere, whereas under stratified conditions, they acted as a CO_2 sink. Morales-Pineda et al. (2014) also reported an important variability of sea-surface pCO_2 on daily, biweekly, and seasonal scales. These studies, among others, emphasize the complexity and the difficulty of hindcasting the preformed, preindustrial DIC of the MS, implying that a more precise estimate of the real air-sea pCO_2 disequilibrium is essential to better assess C^{ant} concentrations.

Applying the MCM and the TrOCA approaches assumes a constant TA. Nevertheless, recent studies (Cossarini et al., 2015; Gemayel et al., 2015) have found a significant seasonal cycle of the surface TA, mainly driven by physical processes (seasonal cycle of evaporation and vertical mixing): variations reach 30 to 50 µmol/kg in the AB. These observations emphasize

the need to use linear regressions, deduced from winter conditions in the Gulf of Lion for deep waters and from the Levantine Basin for intermediate waters. Finally, back-calculation techniques, including TrOCA, require that the MS be in steady state. However, this is not the case, as demonstrated by Schroeder et al. (2008) and Hassoun et al. (2015b). The error associated with this assumption is particularly hard to assess using simple back-calculation techniques. Nevertheless, Touratier et al. (2012) obtained results similar to those of the TrOCA approach by applying the MIX approach that accounts for the contribution of various water masses in the MS.

2.3.3 Anthropogenic carbon inventory

The estimated metrics and C^{ant} inventory for each box are presented in Table 5. According to our results, the AB sequestered between 0.44±0.06 Pg C (MCM) and 0.53±0.06 Pg C (TrOCA) of C^{ant} from the preindustrial era to the summer of 2014. The magnitude of the estimated C^{ant} inventories is explained by the intrinsic characteristics of the western MS (high alkalinity, short water renewal times, active mesoscale structures, etc.) and the increase in atmospheric pCO_2. Palmiéri et al. (2015) proposed that the high TA concentrations of the MS enhance its C^{ant} inventory by 10 % compared to the global ocean. Merlivat et al. (2018) indicated that the accumulated DIC during the last 20 years represents almost 30% of the total inventory of C^{ant} in the MS and that external factors, such as Atlantic inputs, also play an important role in C^{ant} sequestration by the MS. According to Palmiéri et al. (2015), air-sea exchanges alone could explain 75% of the inventory.

The total inventory of C^{ant} in the MS was estimated at 1.7±0.4 Pg C by Schneider et al. (2010) and 1 Pg C by Palmiéri et al. (2015) for 2001. These two inventories were obtained by different techniques (tracer studies and high resolution model, respectively) and for different spatial and temporal scales. It is thus difficult to compare their results with those of this study.

Nevertheless, as Table 6 illustrates, the estimated C^{ant} inventory of the AB is within the range of those reported in many other marginal seas in North Pacific (Chen et al., 2004) and Atlantic (Jutterström et al., 2008; Olsen et al., 2010) Oceans. The AB is characterized by higher average excess CO_2 per unit area (1482-1790 g $C.m^{-2}$) than other marginal seas and oceans because of its intrinsic properties (like low Revelle Factor): e.g., 400 g $C.m^{-2}$ for the Japan Sea (Park et al., 2006), 800 g $C.m^{-2}$ for the Sulu Sea, and 330 g $C.m^{-2}$ for the Global Ocean (Chen et al., 2006a).

Fig. 9 shows the horizontal distribution of the C^{ant} inventory in the AB using the two selected approaches in this study (TrOCA and MCM). The lowest sequestered amounts (9–22 Tg C) are observed in the Sardinian Channel and near Ibiza Island, while the highest correspond with the boxes that have the largest volumes (maximum in box 10 with 74–89 Tg C). These results are consistent with Palmiéri et al. (2015)'s observation of an important correlation with bathymetry. The highest concentrations of C^{ant} per unit volume are observed in the southern and central parts of the AB (0.82 $g.m^{-3}$ (MCM)–0.99 $g.m^{-3}$ (TrOCA)) (Table 5). The inventory maxima encountered at these longitudes possibly reflect the active anticyclonic activity in the area. According to Pessini et al. (2018), the southern part of the basin hosts longer-lived eddies that form and terminate between 4.5 °E and 6.5 °E.

2.4 Acidification estimates and $CaCO_3$ saturation

The difference in pH from the preindustrial era to summer 2014 confirms the high acidification of the AB, with ΔpH values ranging from -0.19 to -0.1 pH unit and a mean value of -0.12±0.008 pH unit (~ -0.0005 pH unit. yr^{-1}) (Table 7). The two approaches used to estimate C^{ant} concentrations yield a similar pH decrease with a mean difference of about 0.01 pH units—almost within the range of the corresponding standard deviations. According to Marcellin Yao et al. (2016), the increasing atmospheric CO_2 accounts for 70% of the decrease

in surface pH at the deep-water formation site while the remaining 30% is caused by increasing seawater temperatures. Fig. 10 illustrates the distribution of ΔpH along the east-west section of the SOMBA cruise, which is strongly correlated with the C^{ant} distribution. The oldest water masses (LIWs) are characterized by the lowest acidification, while the newest are enriched with C^{ant} and are the most acidified waters. The anticyclonic eddy at 6 °E has an acidification of about -0.13 (MCM) to -0.16 pH unit (TrOCA), probably caused by the submesoscale activity mentioned earlier. It is difficult to conclude on the evolution of the acidification based on a comparison of our results with the literature (Hassoun et al., 2015a; Touratier et al., 2012; Touratier and Goyet, 2011) (Table 7). The previous acidification estimates considered the entire MS, while this study focuses solely on the AB, which is more acidified than the MS' eastern basin (e.g., Hassoun et al., 2015a; Touratier and Goyet, 2011).

The saturation states of waters with respect to calcite (Ω_{ca}) and aragonite (Ω_{ar}) are defined by:

$$\Omega_{ca\,(ar)} = \frac{[ca^{2+}]\times[co_3^{2-}]}{K^{*}_{ca\,(ar)}} \qquad (15)$$

where K^* is the stoichiometric solubility product and $[Ca^{2+}]$ and $[CO_3^{2-}]$ are the total calcium and carbonate ion concentrations, respectively.

Variations of the calcite and aragonite saturation states ($\Delta\Omega_{ca}$ and $\Delta\Omega_{ar}$, respectively) were calculated by subtracting the calculated values for the summer of 2014 from the preindustrial values. The mean values of $\Delta\Omega_{Ca}$ and $\Delta\Omega_{ar}$ are -0.9 to -1.06±0.15 for calcite and -0.59 to -0.69±0.09 for aragonite (Table 7). These results are consistent with those of Hassoun et al. (2015a). Nevertheless, despite the important acidification of the basin, Table 7 clearly shows that waters of the AB remain oversaturated with respect to calcite and aragonite throughout its water column, with mean saturation states of 2.4–4.5 and 1.6–2.9, respectively. These results agree with those of Álvarez et al. (2014) and Hassoun et al. (2015a) in the MS, and Chen et al. (2006b) in the South China Sea. In marginal seas, where waters have lower temperatures and

TA than the MS, carbonate mineral undersaturation can be observed below 1000 m (e.g., Chen et al., 1995). Near calcite and aragonite saturation states were observed in the western MS (Ω_{Ca} = 2.5 and Ω_{Ar} = 1.5) during a cruise in 1976 (Millero et al., 1979). According to our results, $CaCO_3$ oversaturation in the MS will probably persist for a few more centuries (Goyet et al., 2016). The increase in the $CaCO_3$ saturation state of waters caused by temperature increase will partly compensate for water acidification as the stoichiometric solubility product of calcium carbonate (K^*) decreases with increasing temperatures caused by global warming, and the faster temperature increase in the MS.

Conclusion

This study, the first to cover the AB in its entirety, was based on a new dataset collected in the summer of 2014 (SOMBA cruise) to better understand the carbonate chemistry and distribution of C^{ant} in the AB. It revealed the influence of biological activity on the distribution patterns of TA and DIC (e.g., photosynthesis and remineralization), in addition to the well-known surface east-west and south-north gradients in the basin. During the summer of 2014, the AB was a source of CO_2 to the atmosphere, but the southwestern part of the basin was a CO_2 sink because of its higher biological activity, as corroborated by the high oxygen concentrations.

The vertical distribution of C^{ant} concentrations is related to the distribution of the main water masses and their respective ages. Nevertheless, this distribution is locally affected by active mesoscale and submesoscale processes in the AB, processes that play an important role in enhancing carbon transport to deep waters. This paper also shows that the two tested approaches (MCM and TrOCA) yield relatively similar C^{ant} distributions and concentration ranges (~50–115 µmol/kg). Nevertheless, the MCM requires a proper parametrization of the preindustrial air-sea disequilibrium because the latter generates high uncertainties on C^{ant}

concentrations estimates in the AB. Moreover, the preindustrial parametrization of DIC ($C^{0,PI}$) has to be assessed more rigorously for deep and intermediate waters, such as by including winter measurements of carbonate system parameters in the area of deep and intermediate water formation.

The sequestered C^{ant} inventory of the AB is about 0.44–0.53±0.06 Pg C (from the preindustrial era to 2014) and is mainly conditioned by the intrinsic characteristics of the MS, the bathymetry, and mesoscale processes in the region (anticyclonic eddies). The accumulation of C^{ant} due to the increasing atmospheric CO_2 concentrations and the quick renewal of deep waters (2005– 2013) caused an acidification ranging from -0.19 to -0.1 pH units. Nevertheless, the AB waters remain oversaturated with respect to calcite and aragonite. This oversaturation will probably persist as the increase of sea surface temperatures partially compensates for the acidification.

Acknowledgments

The SOMBA-GE cruise was the product of an Algerian/French collaboration under the MerMex program, promoted by the I-MOOSE initiative within the framework of MISTRALS. We thank the captains and crew of the R/V Téthys, Benyahia Boudjellal, and Azzouz Mekki for their commitment on-board. We are particularly grateful to the SNAPO-CO_2 laboratory, especially Jonathan Fin, Claire Lo Monaco, and Nicolas Metzl for their high quality measurements. We would also like to thank Dr. Sofiane Soukane for his help on a previous version of the manuscript. Comments from the two anonymous, journal reviewers and Associate Editor Alfonso Mucci helped enhance the quality of the manuscript, we warmly thank them. The SOMBA cruise and geochemical parameter measurements were funded by the French Ministry of foreign affairs (MAEDI) under the ENVIMED program [grant number 2014, 2834-CIRMED].

References

Aït-Ameur, N., Goyet, C., 2006. Distribution and transport of natural and anthropogenic CO_2 in the Gulf of Cádiz. Deep Sea Research Part II: Topical Studies in Oceanography 53, 1329–1343. https://doi.org/10.1016/j.dsr2.2006.04.003

Álvarez, M., Lo Monaco, C., Tanhua, T., Yool, A., Oschlies, A., Bullister, J.L., Goyet, C., Tourtair, F., McDonagh, E., Bryden, H.L., 2009. Estimating the storage of anthropogenic carbon in the subtropical Indian Ocean: A comparison of five different approaches. Biogeosciences (BG) 6, 681–703. https://doi.org/10.5194/bg-6-681-2009

Álvarez, M., Sanleón-Bartolomé, H., Tanhua, T., Mintrop, L., Luchetta, A., Cantoni, C., Schroeder, K., Civitarese, G., 2014. The CO_2 system in the Mediterranean Sea: a basin wide perspective. Ocean Science. 10, 69–92. https://doi.org/10.5194/os-10-69-2014

Anderson, L.A., 1995. On the hydrogen and oxygen content of marine phytoplankton. Deep Sea Research Part I: Oceanographic Research Papers 42, 1675–1680. https://doi.org/10.1016/0967-0637(95)00072-E

Bakun, A., Agostini, V.N., 2001. Seasonal patterns of wind-induced upwelling/downwelling in the Mediterranean Sea. Scientia Marina 65, 243–257.

Bégovic, M., Copin-Montégut, C., 2002. Processes controlling annual variations in the partial pressure of CO_2 in surface waters of the central northwestern Mediterranean Sea (Dyfamed site). Deep Sea Research Part II: Topical Studies in Oceanography 49, 2031–2047.

Benson, B.B., Krause, D., 1984. The concentration and isotopic fractionation of oxygen dissolved in freshwater and seawater in equilibrium with the atmosphere. Limnology and Oceanography 29, 620–632. https://doi.org/10.4319/lo.1984.29.3.0620

Béthoux, J.P., Morin, P., Ruiz-Pino, D.P., 2002. Temporal trends in nutrient ratios: chemical evidence of Mediterranean ecosystem changes driven by human activity. Deep Sea Research Part II: Topical Studies in Oceanography 49, 2007–2016.

Bosse, A., Testor, P., Houpert, L., Damien, P., Prieur, L., Hayes, D., Taillandier, V., Durrieu de Madron, X., d'Ortenzio, F., Coppola, L., Karstensen, J., Mortier, L., 2016. Scales and dynamics of Submesoscale Coherent Vortices formed by deep convection in the northwestern Mediterranean Sea. Journal of Geophysical Research: Oceans 121, 7716–7742. https://doi.org/10.1002/2016JC012144

Chen, C.-T.A., 1993. Carbonate chemistry of the wintertime Bering Sea marginal ice zone. Continental Shelf Research 13, 67–87. https://doi.org/10.1016/0278-4343(93)90036-W

Chen, C.-T.A., Andreev, A., Kim, K.-R., Yamamoto, M., 2004. Roles of Continental Shelves and Marginal Seas in the Biogeochemical Cycles of the North Pacific Ocean. Journal of Oceanography 60, 17–44. https://doi.org/10.1023/B:JOCE.0000038316.56018.d4

Chen, C.-T.A., Hou, W.-P., Gamo, T., Wang, S.L., 2006a. Carbonate-related parameters of subsurface waters in the West Philippine, South China and Sulu Seas. Marine Chemistry, AQUACHEM — 04 99, 151–161. https://doi.org/10.1016/j.marchem.2005.05.008

Chen, C.-T.A., Jones, E.P., Lin, K., 1990. Wintertime total carbon dioxide measurements in the Norwegian and greenland seas. Deep Sea Research Part A. Oceanographic Research Papers 37, 1455–1473. https://doi.org/10.1016/0198-0149(90)90137-K

Chen, G.-T., Millero, F.J., 1979. Gradual increase of oceanic CO_2. Nature 277, 205–206. https://doi.org/10.1038/277205a0

Chen, C.T.A., Tsunogai, S., 1998. Carbon and nutrients in the ocean, in: Asian Change in the Context of Global Climate Change: Impact of Natural and Anthropogenic Changes in Asia on Global Biogeochemical Cycles. pp. 271–307.

Chen, C.-T.A., Wang, S.-L., Bychkov, A.S., 1995. Carbonate chemistry of the Sea of Japan. Journal of Geophysical Research: Oceans 100, 13737–13745. https://doi.org/10.1029/95JC00939

Chen, C.-T.A., Wang, S.-L., Chou, W.-C., Sheu, D.D., 2006b. Carbonate chemistry and projected future changes in pH and $CaCO_3$ saturation state of the South China Sea. Marine Chemistry 101, 277–305. https://doi.org/10.1016/j.marchem.2006.01.007

[dataset] Copernicus Marine Environment Monitoring Service [WWW Document], 2017. Copernicus. URL http://marine.copernicus.eu/services-portfolio/access-to-products/ (accessed 3.20.17).

Copin-Montégut, C., Bégovic, M., 2002. Distributions of carbonate properties and oxygen along the water column (0–2000 m) in the central part of the NW Mediterranean Sea (Dyfamed site): influence of winter vertical mixing on air–sea CO_2 and O_2 exchanges. Deep Sea Research Part II: Topical Studies in Oceanography, Studies at the DYFAMED (France JGOFS) Time-Series Station, N.W. Mediterranean Sea 49, 2049–2066. https://doi.org/10.1016/S0967-0645(02)00027-9

Copin-Montégut, C., Bégovic, M., Merlivat, L., 2004. Variability of the partial pressure of CO_2 on diel to annual time scales in the Northwestern Mediterranean Sea. Marine Chemistry 85, 169–189. https://doi.org/10.1016/j.marchem.2003.10.005

Coppola, L., Legendre, L., Lefèvre, D., Prieur, L., Taillandier, V., Riquier, E.D., 2018. Seasonal and inter-annual variations of dissolved oxygen in the northwestern Mediterranean Sea (DYFAMED site). Progress in Oceanography 162, 187–201.

Cossarini, G., Lazzari, P., Solidoro, C., 2015. Spatiotemporal variability of alkalinity in the Mediterranean Sea. Biogeosciences 12, 1647–1658. https://doi.org/10.5194/bg-12-1647-2015

Dickson, A.G., 1990. Thermodynamics of the dissociation of boric acid in synthetic seawater from 273.15 to 318.15 K. Deep Sea Research Part A. Oceanographic Research Papers 37, 755–766. https://doi.org/10.1016/0198-0149(90)90004-F

Dickson, A.G., Millero, F.J., 1987. A comparison of the equilibrium constants for the dissociation of carbonic acid in seawater media. Deep Sea Research Part A. Oceanographic Research Papers 34, 1733–1743. https://doi.org/10.1016/0198-0149(87)90021-5

Dickson, A.G., Sabine, C.L., Christian, J.R., 2007. Guide to best practices for ocean CO_2 measurements, PICES Special Publication 3. ed, 191 pp.

DOE, 1994. Handbook of Methods for the Analysis of the Various Parameters of the Carbon Dioxide System in Sea Water. Version 2 (No. ORNL/CDIAC-74). A. G. Dickson & C. Goyet, eds. DOI: 10.2172/10107773.

D'Ortenzio, F., Antoine, D., Marullo, S., 2008. Satellite-driven modeling of the upper ocean mixed layer and air–sea CO_2 flux in the Mediterranean Sea. Deep Sea Research Part I: Oceanographic Research Papers 55, 405–434. https://doi.org/10.1016/j.dsr.2007.12.008

Durrieu de Madron, X., Guieu, C., Sempéré, R., Conan, P., Cossa, D., D'Ortenzio, F., Estournel, C., Gazeau, F., Rabouille, C., Stemmann, L., Bonnet, S., Diaz, F., Koubbi, P., Radakovitch, O., Babin, M., Baklouti, M., Bancon-Montigny, C., Belviso, S., Bensoussan, N., Bonsang, B., Bouloubassi, I., Brunet, C., Cadiou, J.-F., Carlotti, F., Chami, M., Charmasson, S., Charrière, B., Dachs, J., Doxaran, D., Dutay, J.-C., Elbaz-Poulichet, F., Eléaume, M., Eyrolles, F., Fernandez, C., Fowler, S., Francour, P., Gaertner, J.C., Galzin, R., Gasparini, S., Ghiglione, J.-F., Gonzalez, J.-L., Goyet, C., Guidi, L., Guizien, K., Heimbürger, L.-E., Jacquet, S.H.M., Jeffrey, W.H., Joux, F., Le Hir, P., Leblanc, K., Lefèvre, D., Lejeusne, C., Lemé, R., Loÿe-Pilot, M.-D., Mallet, M., Méjanelle, L., Melin, F., Mellon, C., Mérigot, B., Merle, P.-L., Migon, C., Miller, W.L., Mortier, L., Mostajir, B., Mousseau, L., Moutin, T., Para, J., Pérez, T., Petrenko, A., Poggiale, J.-C., Prieur, L., Pujo-Pay, M., Pulido-Villena, Raimbault, P., Rees, A.P., Ridame, C., Rontani, J.-F., Ruiz Pino, D., Sicre, M.A., Taillandier, V., Tamburini, C., Tanaka, T., Taupier-Letage, I., Tedetti, M., Testor, P., Thébault, H., Thouvenin, B., Touratier, F., Tronczynski, J., Ulses, C., Van Wambeke, F., Vantrepotte, V., Vaz, S., Verney, R., 2011. Marine ecosystem's responses to climatic and anthropogenic forcings in the Mediterranean. Progress in Oceanography 91, 97–166. https://doi.org/10.1016/j.pocean.2011.02.003

Edmond, J.M., 1970. High precision determination of titration alkalinity and total carbon dioxide content of sea water by potentiometric titration. Deep Sea Research and Oceanographic Abstracts 17, 737–750. https://doi.org/10.1016/0011-7471(70)90038-0

Flecha, S., Pérez, F.F., Navarro, G., Ruiz, J., Olivé, I., Rodríguez-Gálvez, S., Costas, E., Huertas, I.E., 2012. Anthropogenic carbon inventory in the Gulf of Cádiz. Journal of Marine Systems 92, 67–75. https://doi.org/10.1016/j.jmarsys.2011.10.010

Friis, K., 2006. A review of marine anthropogenic CO_2 definitions: introducing a thermodynamic approach based on observations. Tellus B: Chemical and Physical Meteorology 58, 2–15. https://doi.org/10.1111/j.1600-0889.2005.00173.x

Friis, K., Körtzinger, A., Wallace, D.W.R., 2003. The salinity normalization of marine inorganic carbon chemistry data. Geophys. Res. Lett. 30, 1085. https://doi.org/10.1029/2002GL015898

[dataset] GEBCO [WWW Document], 2019. British Oceanographic Data Centre. URL https://www.bodc.ac.uk/data/hosted_data_systems/gebco_gridded_bathymetry_data/ (accessed 3.26.19).

Gemayel, E., Hassoun, A.E.R., Benallal, M.A., Goyet, C., Rivaro, P., Saab, M.A.-A., Krasakopoulou, E., Touratier, F., Ziveri, P., 2015. Climatological variations of total alkalinity

and total inorganic carbon in the Mediterranean Sea surface waters. Earth System Dynamics Discussions 6. https://doi.org/10.5194/esd-6-789-2015

Goyet, C., Davis, D., 1997. Estimation of total CO_2 concentration throughout the water column. Deep Sea Research Part I: Oceanographic Research Papers 44, 859–877. https://doi.org/10.1016/S0967-0637(96)00111-2

Goyet, C., Hassoun, A., Gemayel, E., Touratier, F., Saab, M.A.-A., Guglielmi, V., 2016. Thermodynamic Forecasts of the Mediterranean Sea Acidification. Mediterranean Marine Science 17, 508–518. https://doi.org/10.12681/mms.1487

Gruber, N., Sarmiento, J.L., Stocker, T.F., 1996. An improved method for detecting anthropogenic CO_2 in the oceans. Global Biogeochemical Cycles 10, 809–837. https://doi.org/10.1029/96GB01608

Hainbucher, D., Rubino, A., Cardin, V., Tanhua, T., Schroeder, K., Bensi, M., 2014. Hydrographic situation during cruise M84/3 and P414 (spring 2011) in the Mediterranean Sea. Ocean Sci. 10, 669–682. https://doi.org/10.5194/os-10-669-2014

Hassoun, A.E.R., Gemayel, E., Krasakopoulou, E., Goyet, C., Abboud-Abi Saab, M., Guglielmi, V., Touratier, F., Falco, C., 2015a. Acidification of the Mediterranean Sea from anthropogenic carbon penetration. Deep Sea Research Part I: Oceanographic Research Papers 102, 1–15. https://doi.org/10.1016/j.dsr.2015.04.005

Hassoun, A.E.R., Gemayel, E., Krasakopoulou, E., Goyet, C., Saab, M.A.-A., Ziveri, P., Touratier, F., Guglielmi, V., Falco, C., 2015b. Modeling of the Total Alkalinity and the Total Inorganic Carbon in the Mediterranean Sea. Journal of Water Resources and Ocean Science 24–32. https://doi.org/10.11648/j.wros.20150401.14

Hood, E.M., Merlivat, L., 2001. Annual to interannual variations of fCO_2 in the northwestern Mediterranean Sea: Results from hourly measurements made by CARIOCA buoys, 1995-1997. Journal of Marine Research 59, 113–131. https://doi.org/10.1357/002224001321237399

Houpert, L., 2013. Contributions to the Study of Transfer Processes from the Surface to the Deep Ocean in the Mediterranean Sea using in situ Measurements (thesis). Université de Perpignan Via Domitia, France.

Huertas, I.E., Ríos, A.F., García-Lafuente, J., Makaoui, A., Rodríguez-Gálvez, S., Sánchez-Román, A., Orbi, A., Ruíz, J., Pérez, F.F., 2009. Anthropogenic and natural CO_2 exchange through the Strait of Gibraltar. Biogeosciences 6, 647–662. https://doi.org/10.5194/bg-6-647-2009

Jutterström, S., Jeansson, E., Anderson, L.G., Bellerby, R., Jones, E.P., Smethie, W.M., Swift, J.H., 2008. Evaluation of anthropogenic carbon in the Nordic Seas using observed relationships of N, P and C versus CFCs. Progress in Oceanography 78, 78–84. https://doi.org/10.1016/j.pocean.2007.06.001

[dataset] Kanamitsu, M., Ebisuzaki, W., Woollen, J., Yang, S.-K., Hnilo, J.J., Fiorino, M., Potter, G.L., 2002. NCEP-DOE AMIP-II Reanalysis (R-2).

Kessouri, F., Ulses, C., Estournel, C., Marsaleix, P., D'Ortenzio, F., Severin, T., Taillandier, V., Conan, P., 2018. Vertical Mixing Effects on Phytoplankton Dynamics and Organic Carbon Export in the Western Mediterranean Sea. Journal of Geophysical Research: Oceans 123, 1647–1669. https://doi.org/10.1002/2016JC012669

Körtzinger, A., Hedges, J.I., Quay, P.D., 2001. Redfield ratios revisited: Removing the biasing effect of anthropogenic CO_2. Limnology and Oceanography 46, 964–970. https://doi.org/10.4319/lo.2001.46.4.0964

La Ferla, R., Azzaro, M., Civitarese, G., Ribera d'Alcalà, M., 2003. Distribution patterns of carbon oxidation in the eastern Mediterranean Sea: Evidence of changes in the remineralization processes. J. Geophys. Res. 108, 8111. https://doi.org/10.1029/2002JC001602

Langdon, C., 2010. Determination of dissolved oxygen in seawater by Winkler titration using the amperometric technique (No. IOCCP Report Number 14. IOCCP Publication Series Number 134). The GOSHIP Repeat Hydrography Manual: a Collection of Expert Reports and Guidelines, edited by: Hood, EM, Sabine, CL, and Sloyan, BM.

Lee, K., Sabine, C.L., Tanhua, T., Kim, T.-W., Feely, R.A., Kim, H.-C., 2011. Roles of marginal seas in absorbing and storing fossil fuel CO_2. Energy Environ. Sci. 4, 1133–1146. https://doi.org/10.1039/C0EE00663G

Lee, K., Tong, L.T., Millero, F.J., Sabine, C.L., Dickson, A.G., Goyet, C., Park, G.-H., Wanninkhof, R., Feely, R.A., Key, R.M., 2006. Global relationships of total alkalinity with salinity and temperature in surface waters of the world's oceans. Geophys. Res. Lett. 33, L19605. https://doi.org/10.1029/2006GL027207

Lo Monaco, C., Metzl, N., Poisson, A., Brunet, C., Schauer, B., 2005. Anthropogenic CO_2 in the Southern Ocean: Distribution and inventory at the Indian-Atlantic boundary (World Ocean Circulation Experiment line I6). Journal of Geophysical Research: Oceans 110. https://doi.org/10.1029/2004JC002643

Louanchi, F., Boudjakdji, M., Nacef, L., 2009. Decadal changes in surface carbon dioxide and related variables in the Mediterranean Sea as inferred from a coupled data-diagnostic model approach. ICES J Mar Sci 66, 1538–1546. https://doi.org/10.1093/icesjms/fsp049

Lovato, T., Vichi, M., 2015. An objective reconstruction of the Mediterranean Sea carbonate system. Deep Sea Research Part I: Oceanographic Research Papers 98, 21–30. https://doi.org/10.1016/j.dsr.2014.11.018

Malanotte-Rizzoli, P., Artale, V., Borzelli-Eusebi, G.L., Brenner, S., Crise, A., Gacic, M., Kress, N., Marullo, S., Ribera d'Alcalà, M., Sofianos, S., Tanhua, T., Theocharis, A., Alvarez, M., Ashkenazy, Y., Bergamasco, A., Cardin, V., Carniel, S., Civitarese, G., D'Ortenzio, F., Font, J., Garcia-Ladona, E., Garcia-Lafuente, J.M., Gogou, A., Gregoire, M., Hainbucher, D., Kontoyannis, H., Kovacevic, V., Kraskapoulou, E., Kroskos, G., Incarbona, A., Mazzocchi, M.G., Orlic, M., Ozsoy, E., Pascual, A., Poulain, P.-M., Roether, W., Rubino, A., Schroeder, K., Siokou-Frangou, J., Souvermezoglou, E., Sprovieri, M., Tintoré, J., Triantafyllou, G., 2014. Physical forcing and physical/biochemical variability of the Mediterranean Sea: a

review of unresolved issues and directions for future research. Ocean Science 10, 281–322. https://doi.org/10.5194/os-10-281-2014

Marcellin Yao, K., Marcou, O., Goyet, C., Guglielmi, V., Touratier, F., Savy, J.-P., 2016. Time variability of the north-western Mediterranean Sea pH over 1995–2011. Marine Environmental Research 116, 51–60. https://doi.org/10.1016/j.marenvres.2016.02.016

Mehrbach, C., Culberson, C.H., Hawley, J.E., Pytkowicx, R.M., 1973. Measurement of the Apparent Dissociation Constants of Carbonic Acid in Seawater at Atmospheric Pressure 1. Limnol. Oceanogr. 18, 897–907. https://doi.org/10.4319/lo.1973.18.6.0897

Merlivat, L., Boutin, J., Antoine, D., Beaumont, L., Golbol, M., Vellucci, V., 2018. Increase of dissolved inorganic carbon and decrease in pH in near-surface waters in the Mediterranean Sea during the past two decades. Biogeosciences 15, 5653–5662. https://doi.org/10.5194/bg-15-5653-2018

Millero, F.J., Lee, K., Roche, M., 1998. Distribution of alkalinity in the surface waters of the major oceans. Marine Chemistry 60, 111–130. https://doi.org/10.1016/S0304-4203(97)00084-4

Millero, F.J., Morse, J., Chen, C.-T., 1979. The carbonate system in the western Mediterranean Sea. Deep Sea Research Part A. Oceanographic Research Papers 26, 1395–1404. https://doi.org/10.1016/0198-0149(79)90007-4

Millot, C., Taupier-Letage, I., 2005. Circulation in the Mediterranean Sea, in: Saliot, A. (Ed.), The Mediterranean Sea, Handbook of Environmental Chemistry. Springer Berlin Heidelberg, pp. 29–66. https://doi.org/10.1007/b107143

Morales-Pineda, M., Cózar, A., Laiz, I., Úbeda, B., Gálvez, J.Á., 2014. Daily, biweekly, and seasonal temporal scales of pCO_2 variability in two stratified Mediterranean reservoirs. Journal of Geophysical Research: Biogeosciences 119, 509–520. https://doi.org/10.1002/2013JG002317

[dataset] Mortier, L., Aït-Ameur, N., Taillandier, V., 2014. SOMBA-GE-2014 cruise, Téthys II R/V. https://doi.org/10.17600/14007500

Moutin, T., Prieur, L., 2012. Influence of anticyclonic eddies on the biogeochemistry from the Oligotrophic to the ultraoligotrophic Mediterranean (BOUM cruise). Biogeosciences 9, 3827–3855. https://doi.org/10.5194/bg-9-3827-2012

Olsen, A., Omar, A.M., Jeansson, E., Anderson, L.G., Bellerby, R.G.J., 2010. Nordic seas transit time distributions and anthropogenic CO_2. Journal of Geophysical Research: Oceans 115. https://doi.org/10.1029/2009JC005488

Palmiéri, J., Orr, J.C., Dutay, J.-C., Béranger, K., Schneider, A., Beuvier, J., Somot, S., 2015. Simulated anthropogenic CO_2 storage and acidification of the Mediterranean Sea. Biogeosciences (BG) 12, 781–802. https://doi.org/10.5194/bg-12-781-2015

Park, G.-H., Lee, K., Tishchenko, P., Min, D.-H., Warner, M.J., Talley, L.D., Kang, D.-J., Kim, K.-R., 2006. Large accumulation of anthropogenic CO_2 in the East (Japan) Sea and its

significant impact on carbonate chemistry. Global Biogeochemical Cycles 20. https://doi.org/10.1029/2005GB002676

Pessini, F., Olita, A., Cotroneo, Y., Perilli, A., 2018. Mesoscale eddies in the Algerian Basin: do they differ as a function of their formation site? Ocean Science 14, 669–688. https://doi.org/10.5194/os-14-669-2018

Pierrot, D., Lewis, E., Wallace, D.W.R., 2006. MS Excel Program Developed for CO_2 System Calculations. ORNL/CDIAC-105a. doi: 10.3334/CDIAC/otg.COSYS_XLS_CDIAC105a.

Puig, P., Salat, J., Martín, J., Palanques, A., Emelianov, M., 2013. Thick bottom nepheloid layers in the western Mediterranean generated by deep dense shelf water cascading. https://doi.org/10.1016/j.pocean.2012.10.003

Rivaro, P., Messa, R., Massolo, S., Frache, R., 2010. Distributions of carbonate properties along the water column in the Mediterranean Sea: Spatial and temporal variations. Marine Chemistry 121, 236–245. https://doi.org/10.1016/j.marchem.2010.05.003

Sabine, C.L., Tanhua, T., 2010. Estimation of Anthropogenic CO_2 Inventories in the Ocean. Annual Review of Marine Science 2, 175–198. https://doi.org/10.1146/annurev-marine-120308-080947

SBE, 2010. SBE 43 Dissolved Oxygen Sensor Calibration and Data Corrections using Winkler Titrations (APPLICATION NOTE No. 64-2). Sea-Bird Electronics, Inc., 13431 NE 20th Street Bellevue, WA 98005, USA.

Schlitzer, R., Ocean Data View, odv.awi.de, 2018

Schneider, A., Tanhua, T., Körtzinger, A., Wallace, D.W.R., 2010. High anthropogenic carbon content in the eastern Mediterranean. J. Geophys. Res. 115, C12050. https://doi.org/10.1029/2010JC006171

Schroeder, K., Josey, S.A., Hermann, M., Grignon, L., Gasparini, G.P., Bryden, H.L., 2010. Abrupt warming and salting of the Western Mediterranean Deep Water after 2005: Atmospheric forcings and lateral advection. Journal of Geophysical Research 115. https://doi.org/10.1029/2009JC005749

Schroeder, K., Ribotti, A., Borghini, M., Sorgente, R., Perilli, A., Gasparini, G.P., 2008. An extensive western Mediterranean deep water renewal between 2004 and 2006. Geophys. Res. Lett. 35, L18605. https://doi.org/10.1029/2008GL035146

Sisma-Ventura, G., Yam, R., Kress, N., Shemesh, A., 2016. Water column distribution of stable isotopes and carbonate properties in the South-eastern Levantine basin (Eastern Mediterranean): Vertical and temporal change. Journal of Marine Systems 158, 13–25. https://doi.org/10.1016/j.jmarsys.2016.01.012

Swift, J.H., 2010. Reference-quality water sample data: notes on acquisition, record keeping, and evaluation (The GO-SHIP Repeat Hydrography Manual: A collection of expert Reports and Guidlines No. IOCCP Report N14).

Taillandier, V., D'Ortenzio, F., Antoine, D., 2012. Carbon fluxes in the mixed layer of the Mediterranean Sea in the 1980s and the 2000s. Deep Sea Research Part I: Oceanographic Research Papers 65, 73–84. https://doi.org/10.1016/j.dsr.2012.03.004

Testor, P., Gascard, J.C., 2003. Large-scale spreading of deep waters in the Western Mediterranean Sea by submesoscale coherent eddies. Journal of physical oceanography 33, 75–87. https://doi.org/10.1175/1520-0485(2003)033<0075:LSSODW>2.0.CO;2

Testor, P., Send, U., Gascard, J.-C., Millot, C., Taupier-Letage, I., Béranger, K., 2005. The mean circulation of the southwestern Mediterranean Sea: Algerian Gyres. J. Geophys. Res. 110, C11017. https://doi.org/10.1029/2004JC002861

Touratier, F., Azouzi, L., Goyet, C., 2007. CFC-11, ^{14}C and ^{3}H tracers as a means to assess anthropogenic CO_2 concentrations in the ocean. Tellus B 59, 318–325. https://doi.org/10.1111/j.1600-0889.2006.00247.x

Touratier, F., Goyet, C., 2004. Applying the new TrOCA approach to assess the distribution of anthropogenic CO_2 in the Atlantic Ocean. Journal of Marine Systems 46, 181–197. https://doi.org/10.1016/j.jmarsys.2003.11.020

Touratier, F., Goyet, C., 2011. Impact of the Eastern Mediterranean Transient on the distribution of anthropogenic CO_2 and first estimate of acidification for the Mediterranean Sea. Deep Sea Research Part I: Oceanographic Research Papers 58, 1–15. https://doi.org/10.1016/j.dsr.2010.10.002

Touratier, F., Goyet, C., 2009. Decadal evolution of anthropogenic CO_2 in the northwestern Mediterranean Sea from the mid-1990s to the mid-2000s. Deep Sea Research Part I: Oceanographic Research Papers 56, 1708–1716. https://doi.org/10.1016/j.dsr.2009.05.015

Touratier, F., Goyet, C., Houpert, L., de Madron, X.D., Lefèvre, D., Stabholz, M., Guglielmi, V., 2016. Role of deep convection on anthropogenic CO_2 sequestration in the Gulf of Lions (northwestern Mediterranean Sea). Deep Sea Research Part I: Oceanographic Research Papers 113, 33–48. https://doi.org/10.1016/j.dsr.2016.04.003

Touratier, F., Guglielmi, V., Goyet, C., Prieur, L., Pujo-Pay, M., Conan, P., Falco, C., 2012. Distributions of the carbonate system properties, anthropogenic CO_2, and acidification during the 2008 BOUM cruise (Mediterranean Sea). Biogeosciences Discussions 9, 2709–2753. https://doi.org/10.5194/bgd-9-2709-2012

Tréguer, P., LeCorre, P., 1975. Manuel d'analyse des sels nutritifs dans l'eau de mer. Utilisation de l'AutoAnalyser II Technicon, 2nd ed. ed. Univ. Bretagne Occidentale, Laboratoire de Chimie marine, Brest, France.

Uppström, L.R., 1974. The boron/chlorinity ratio of deep-sea water from the Pacific Ocean. Deep Sea Research and Oceanographic Abstracts 21, 161–162. https://doi.org/10.1016/0011-7471(74)90074-6

Vázquez-Rodríguez, M., Touratier, F., Lo Monaco, C., Waugh, D.W., Padin, X.A., Bellerby, R.G.J., Goyet, C., Metzl, N., Ríos, A.F., Pérez, F.F., 2009. Anthropogenic carbon distributions in the Atlantic Ocean: data-based estimates from the Arctic to the Antarctic. Biogeosciences 6, 439–451. https://doi.org/10.5194/bg-6-439-2009

[dataset] WDCGG [WWW Document], 2018. World Data Centre for Greenhous Gases. URL https://gaw.kishou.go.jp/ (accessed 4.23.18).

Weiss, R.F., Price, B.A., 1980. Nitrous oxide solubility in water and seawater. Marine Chemistry 8, 347–359. https://doi.org/10.1016/0304-4203(80)90024-9

Yool, A., Oschlies, A., Nurser, A.J.G., Gruber, N., 2010. A model-based assessment of the TrOCA approach for estimating anthropogenic carbon in the ocean. Biogeosciences 7, 723–751. https://doi.org/10.5194/bg-7-723-2010

Figures captions

Fig. 1: The distribution of SOMBA cruise stations (white dots correspond to the sampled stations for TA/DIC). The base map represents the Mediterranean Sea gridded Sea Level Anomaly all-sat-merged (L4), expressed in meters for August 16, 2014. Downloaded from Copernicus Marine Environment Monitoring Service website ("Copernicus Marine Environment Monitoring Service," 2017). **(color should be used for this figure in print)**

Fig. 2: Vertical variability of Total Alkalinity (a) and Dissolved Inorganic Carbon (b) residuals using the proposed equations. SDr is the Standard Deviation of the residuals. **(color should not be used for this figure in print)**

Fig. 3: Theta/Practical Salinity (θ/S_p) diagrams for the entire water column (a); the intermediate layer (b); the deep layer (c). The color bar scales depict longitude in degrees for (a) and (b), and Apparent Oxygen Utilization for (c). (d) is the vertical distribution of salinity along an east-west section during the SOMBA cruise. AW/MAW: Atlantic Waters/Modified Atlantic Waters; LIW: Levantine Intermediate Waters; WIW: Winter Intermediate Waters; WMDW: Western Mediterranean Deep Waters; WMDWn: newly formed Western Mediterranean Deep Waters. **(color should be used for this figure in print)**

Fig. 4: Boxplots of TA (a), DIC (b), pH_T (c) and pCO_2 (d) for the SOMBA cruise data over three depth layers (surface, intermediate, and deep). The box limits correspond to the first quartile, median, and third quartile, respectively; the straight line represents the minimum and maximum; the black dots are the outliers; the diamond dots correspond to the mean values. **(color should not be used for this figure in print)**

Fig. 5: Surface distribution of TA (a), salinity-normalized TA (b), DIC (c), salinity-normalized DIC (d), pH_T (e), ΔpCO_2 (f), oxygen saturation (g) and practical salinity (h) during the SOMBA cruise. **(color should be used for this figure in print)**

Fig. 6: The vertical distributions of the non-normalized and salinity-normalized TA (a and b, respectively) and DIC (c and d, respectively) along an east-west section during the SOMBA cruise. **(color should be used for this figure in print)**

Fig. 7: The mean longitudinal (a, b, c, d) and latitudinal (e, f, g, h) evolution of the non-normalized and normalized TA and DIC concentrations, respectively, for the surface, intermediate, and deep layers. The error bars correspond with the standard deviation and the dashed line is the mean linear trend with its confidence interval (in gray). **(color should not be used for this figure in print)**

Fig. 8: The vertical distribution along an east-west section of: (a) anthropogenic carbon concentration computed by the TrOCA approach; (b) anthropogenic carbon concentration computed by the MCM; (c) Apparent Oxygen Utilization **(color should be used for this figure in print)**

Fig. 9: The distribution of anthropogenic carbon inventory in the Algerian Basin using two approaches; the TrOCA (orange) and the MCM (yellow). The numbers correspond to box identification numbers and the blue scale bar to bathymetry. **(color should not be used for this figure in print)**

Fig. 10: East-west vertical distribution of ΔpH computed using anthropogenic carbon concentration values of the MCM (a) and the TrOCA (b) approaches. **(color should be used for this figure in print)**

Table 1: Monthly mean atmospheric carbon dioxide dry air mole fraction for the selected stations for CO_2 survey for August and September 2014

Measurement stations_code_country	**Location (lat/long)**	**Sampling altitude (m)**	**Monthly mean xCO_2 values (ppm) ± uncertainty (SD)**	
			17-31 August	**01-08 September**
Monte Cimone_ CMN_Italy	44.16°E/10.68°E	2177	388.55±2.22	391.51±2.21
Plateau Rosa_PRS_Italy	45.93°N/7.7°E	3490	390.62±0.54	391.37±0.96
Puy du dome_ PUY_France	45.77°N/2.96	1475	387.82±2.88	393.32±2.16
Lampedusa_LMP_Italy	35.52°N/12.62°E	50	390.24±2.25	395.09±0.02
Assekrem_ASK_Algeria	23.26°N/5.63°E	2715	393.93±0.64	394.75±0.14
Begure_BGU_Spain	3.23°E/41.97°N	13	391.81±3.51	398.32
Mean (all data)			**390±2.8 N=56 values**	**393±2.4 N=23 values**

SD: Standard Deviation

N=number of considered measurements to compute the mean

Table 2: The estimated errors related to anthropogenic carbon calculation using the Modified Chen and Millero approach (MCM)

Error (σ)	Value	Assessment method
σ_{O_2}	1.6 µmol/kg	Measurement precision of dissolved oxygen
$\sigma_{O_2^0}$	4.9 µmol/kg	RMSD of the preformed oxygen estimated between the selected and the sensitivity test's parametrization (Table 3.1)
σ_{TA}	2 µmol/kg	Measurement precision of Total Alkalinity
σ_{TA^0}	7.5 µmol/kg	RMSD of equation 11
σ_{DIC}	3.3 µmol/kg	Measurement precision of Dissolved Inorganic Carbon
$\sigma_{C^{0,PI}}$	3 µmol/kg	The error is deduced by the method of Gruber et al. (1996), by considering a multi-parametric linear regression of $C^{0,PI}$ ($C^{0,PI}$=68.517 S_p -10.707 θ+0.004 AOU - 270.013), based on the SOMBA data. The considered error is the residual between the directly calculated and the linearized $C^{0,PI}$ ($RMSD_{mean}$=1.5 µmol/kg; $RMSD_{max}$= 5 µmol/kg)
$\sigma_{\frac{C}{O_2}}$	0.0816	The error is estimated by error propagation of the uncertainties on C, N and O_2, given by Anderson (1995)
$\sigma_{\frac{N}{O_2}}$	0.0097	

O_2: dissolved oxygen; O_2^0: preformed dissolved oxygen; TA: Total Alkalinity; TA^0: preformed preindustrial Total Alkalinity; DIC: Dissolved Inorganic Carbon; $C^{0,PI}$: preformed preindustrial DIC; C/O_2 and N/O_2: Molar ratios; RMSD: Root Mean Square Deviation

Table 3: (1) Root Mean Square Deviation (RMSD) between the values of the selected and the sensitivity tests' parametrizations for the parameters O_2^0, TA^0, and $C^{0,PI}$; (2) RMSD of anthropogenic carbon values between the selected and the sensitivity tests' parametrizations.

		Molar Ratio	O_2^0	TA^0_1	TA^0_2	TA^0_mean	$C^{0,PI}$
1	**RMSD of the parameters (µmol/kg)**	-	4.87	5.05	16.59	10.51	9.38
	N	-	1013	1022	1022	1022	618
2	**RMSD of C^{ant} (µmol/kg)**	2.2	3.8	0.98	5.27	3.1	9.35
	N	618	618	618	618	618	618

N is the number of the considered values; O_2^0 is the preformed, preindustrial oxygen; TA^0_1 and TA^0_2 are the tested preformed, preindustrial Alkalinities deduced from the proposed equations of Hassoun et al. (2015b), and Copin-Montégut and Bégovic (2002), respectively. TA^0_mean is the mean value of TA^0_1 and TA^0_2; $C^{0,PI}$ is the preformed, preindustrial DIC

Table 4: Descriptive statistics on anthropogenic carbon concentrations using the TrOCA and the MCM approaches in addition to sensitivity tests results (sen1: preformed oxygen; sen2: molar ratios; sen3 and 4: preformed TA; sen5: air-sea disequilibrium)

	C^{ant} TrOCA (µmol/kg)	C^{ant} MCM (µmol/kg)	C^{ant}_sen1 (µmol/kg)	C^{ant}_ sen2 (µmol/kg)	C^{ant}_ sen3 (µmol/kg)	C^{ant}_ sen4 (µmol/kg)	C^{ant}_ sen5 (µmol/kg)
Min.	61	50	46	47	50	55	40
Mean	81	69	65	67	70	74	59
SD	4.3	5.2	5.2	5.2	5.3	5.2	5.2
Max.	115	109	105	108	111	114	100

Min: Minimum, Max: Maximum, SD: Standard Deviation

Table 5: Metrics on anthropogenic carbon inventory boxes (surfaces and volumes) and the corresponding sequestered carbon in g/m^3 and Teragram of carbon (Tg C) for the TrOCA and the MCM approaches

Box	Lat.	Long.	Volume (m^3)	Surface (km^2)	Avr. Depth (m)	C^{ant} TrOCA ($g\ C/m^3$)	C^{ant} TrOCA (Tg C)	C^{ant} MCM ($g\ C/m^3$)	C^{ant} MCM (Tg C)
1	37	-1	5,84. 10^{13}	30058	1812±997	0.94	55.36	0.78	45.73
2	37	1	7,12. 10^{13}	30935	2377±700	0.93	65.94	0.76	54.32
3	37	3	5,67. 10^{13}	23865	2407±795	0.94	53.56	0.78	44.29
4	37	5	5,34. 10^{13}	22508	2425±735	0.94	50.06	0.78	41.44
5	37	7	4,42. 10^{13}	18915	2291±945	0.99	43.52	0.82	36.23
6	37	9	1,29. 10^{13}	12840	853±963	0.9	11.64	0.75	9.62
7	39	1	1,12. 10^{13}	13830	764±597	0.92	10.24	0.77	8.55
8	39	3	4,72. 10^{13}	26018	1743±991	0.94	44.36	0.78	36.63
9	39	5	9,06. 10^{13}	37527	2535±585	0.94	85.46	0.78	70.60
10	39	7	9,48. 10^{13}	38393	2618±585	0.94	88.8	0.78	73.6
11	39	9	2,42. 10^{13}	21751	1014±820	0.9	21.88	0.75	18.28

Table 6: Comparison of anthropogenic carbon inventory in different marginal seas (Pg C: Petagram of Carbon)

Marginal Seas	Year	C^{ant} inventory (Pg C)	Surface ($\times 10^6$ km^2)	Calculation method	Reference
Mediterranean Sea	2001	1.7±0.4	2.5	TTD	(Schneider et al., 2010)
	2001	1		Regional Model	(Palmiéri et al., 2015)
Algerian Basin	**2014**	**0.44-0.53±0.06**	**0.28**	**Chen and Millero (1979) and TrOCA**	**Current study**
Bering Sea	1980	0.21±0.05	1.1	Chen and Millero (1979)	(Chen, 1993)
Okhotsk Sea	1998	0.18±0.08	1.01	Chen and Millero (1979)	(Chen and Tsunogai, 1998)
Japan Sea	1992	0.31±0.05	0.74	Chen and Millero (1979)	(Chen et al., 1995)
	1999	0.40 ± 0.06		Tracer based technique (chlorofluorocarbon)	(Park et al., 2006)
East China and Yellow Seas	1992	0.07±0.02	0.9	Chen and Millero (1979)	(Chen et al., 2004)
South China Sea	1999	0.6±0.15	1.1	Chen and Millero (1979)	(Chen et al., 2006b)
Sulu Sea	1996	0.28	0.35	Chen and Millero (1979)	(Chen et al., 2006a)
Nordic Seas (Norwegian and Greenland Seas)	1990	0.85	~ 2.6	Chen and Millero (1979)	(Chen et al., 1990)
	2002	1.2		Method combining nutrients and CFC data	(Jutterström et al., 2008)
	2002	0.9-1.4		TTD	(Olsen et al., 2010)

Table 7: The Mean variation of pH and seawater saturation states in regards to calcite ($\Delta\Omega_{Ca}$) and aragonite ($\Delta\Omega_{Ar}$), between the preindustrial era and the summer of 2014. The table shows the results considering the anthropogenic carbon computed by both the TrOCA and the MCM approaches.

Parameter	Min.	Mean value	Max.	SD
ΔpH_{MCM}	-0.19	-0.115	-0.083	± 0.008
ΔpH_{TrOCA}	-0.199	-0.134	-0.101	± 0.007
Ω_{Ca} 2014	2.414	3.806	4.514	± 0.501
Ω_{Ar} 2014	1.603	2.464	2.909	± 0.306
Ω_{Ca} preind (MCM)	3.143	4.712	5.764	± 0.644
$\Delta\Omega_{Ca}$ (Chen)	**-1.564**	**-0.907**	**-0.567**	**± 0.156**
Ω_{Ca} preind (TrOCA)	3.307	4.868	5.816	± 0.639
$\Delta\Omega_{Ca}$ (TrOCA)	**-1.644**	**-1.063**	**-0.722**	**± 0.149**
Ω_{Ar} preind (MCM)	2.087	3.051	3.718	±0.394
$\Delta\Omega_{Ar}$ (MCM)	**-1.008**	**-0.587**	**-0.376**	**± 0.097**
Ω_{Ar} preind (TrOCA)	2.197	3.152	3.747	± 0.39
$\Delta\Omega_{Ar}$ (TrOCA)	**-1.06**	**-0.668**	**-0.479**	**± 0.091**
Previous studies (Mediterranean Sea)				
ΔpH_{2001}^{TrOCA} (Touratier and Goyet, 2011)	-0.05	-	0.14	-
ΔpH_{2001}^{Model} (Palmiéri et al., 2015)	-0,06	-	-0,005	-
ΔpH_{2008}^{TrOCA} (Touratier et al., 2012)	-0,148	-	-0,061	-
ΔpH_{2013}^{TrOCA} (Hassoun et al., 2015a)	0.156	-	-0.055	-

SD: Standard deviation; N=618: number of considered data

Highlights:

- The first high resolution spatial coverage of the Algerian Basin allowed a detailed study of the carbonate system parameters using a new dataset (SOMBA 2014: Système d'Observations à la mer dans le Bassin Algérien).

- A refitted back-calculation method of anthropogenic carbon that considers the characteristics of the Mediterranean Sea displays similar results to the well-known TrOCA method.

- Highlighting of the role of the neglected submesoscale processes, correlated with mesoscale activity, in the increase of anthropogenic carbon sequestration.

- The estimated acidification of the Algerian Basin from the preindustrial era to 2014 range between -0.19 and -0.1 pH unit.

- The first estimate of the anthropogenic carbon inventory trapped by the Algerian Basin using *in situ* data is about 0.44-0.53±0.06 Pg C in 2014.

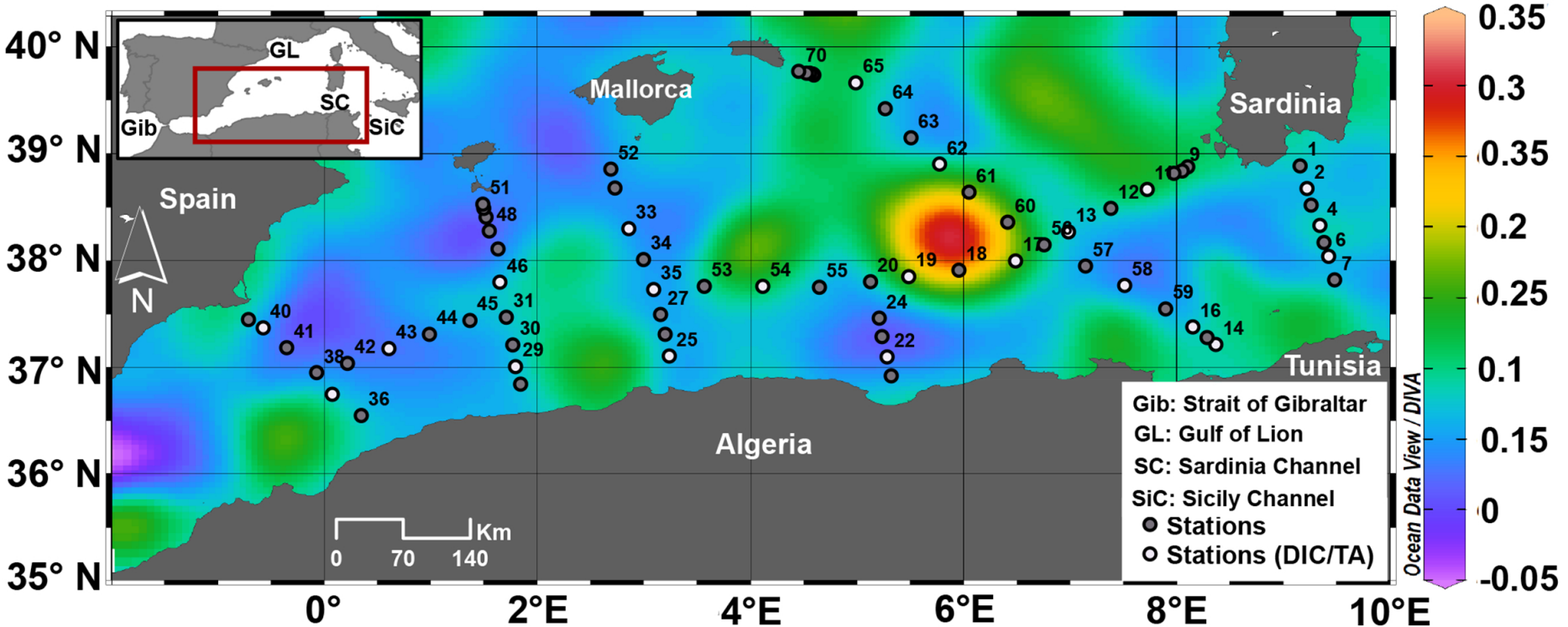
GL
SC
Gib
SiC
Spain
Mallorca
Sardinia
Tunisia
Algeria
N
Km
0
70
140
Gib: Strait of Gibraltar
GL: Gulf of Lion
SC: Sardinia Channel
SiC: Sicily Channel
Stations
Stations (DIC/TA)
Ocean Data View / DIVA
0.35
0.3
0.35
0.2
0.25
0.1
0.15
0
-0.05
40° N
39° N
38° N
37° N
36° N
35° N
0°
2°E
4°E
6°E
8°E
10°E

Figure 1

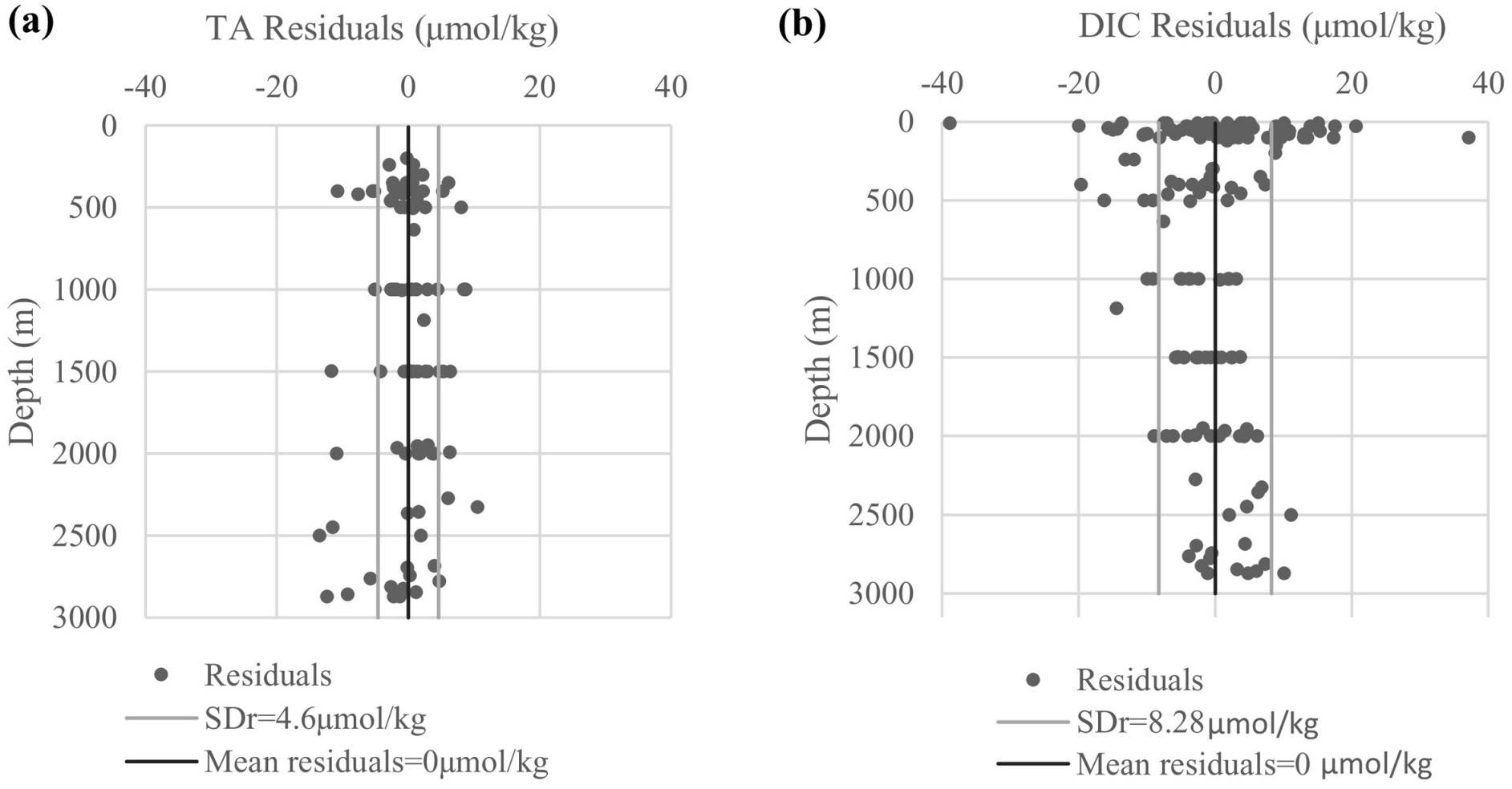
(a)
TA Residuals (µmol/kg)
-40
-20
0
20
40
0
500
1000
1500
2000
2500
3000
Depth (m)
Residuals
SDr=4.6µmol/kg
Mean residuals=0µmol/kg
(b)
DIC Residuals (µmol/kg)
-40
-20
0
20
40
0
500
1000
1500
2000
2500
3000
Depth (m)
Residuals
SDr=8.28µmol/kg
Mean residuals=0 µmol/kg

Figure 2

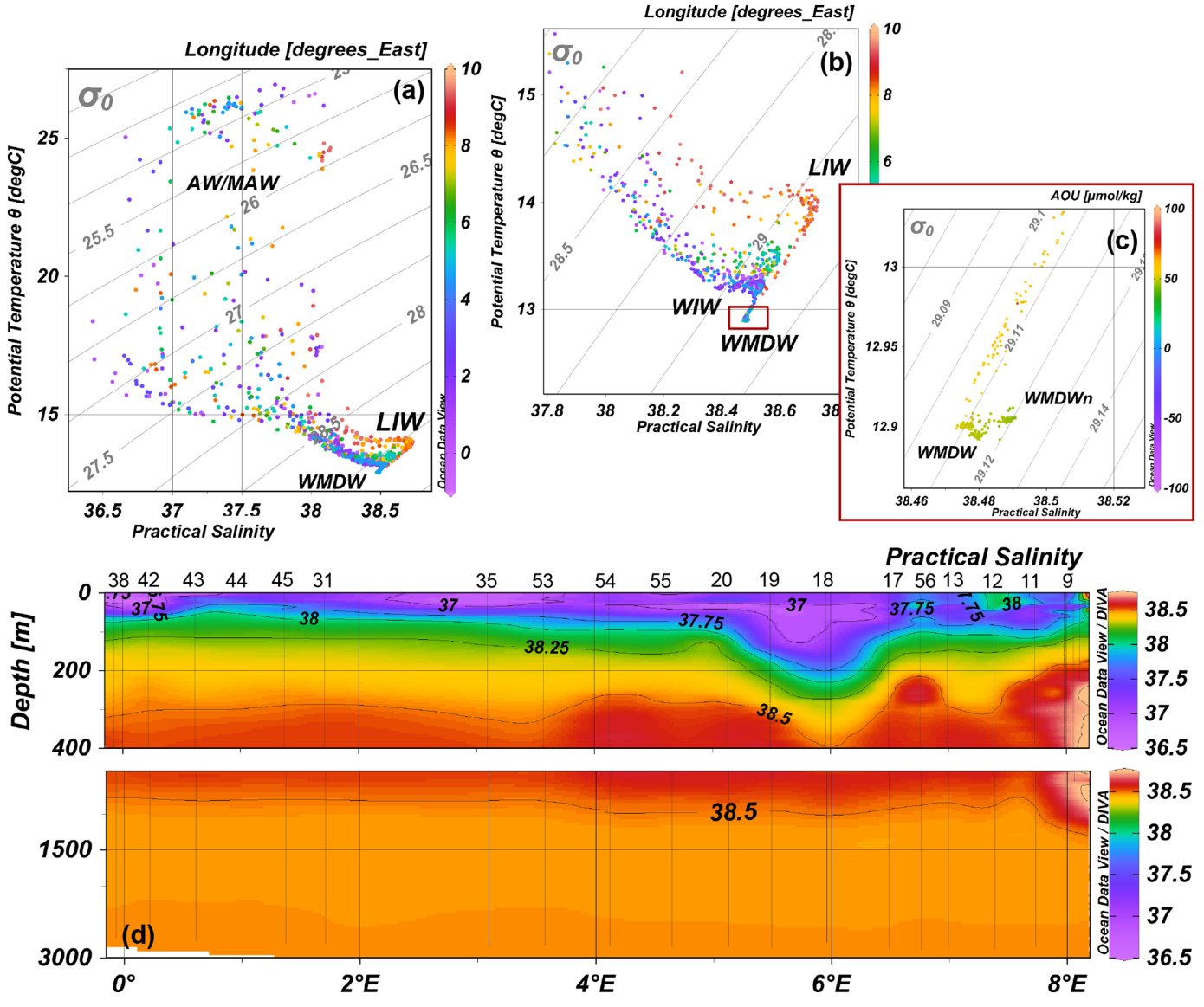
Longitude [degrees_East]
σ0
(a)
AW/MAW
LIW
WMDW
Potential Temperature θ [degC]
Practical Salinity
Ocean Data View
(b)
WIW
(c)
AOU [µmol/kg]
WMDWn
Practical Salinity
Depth [m]
(d)
Ocean Data View / DIVA

Figure 3

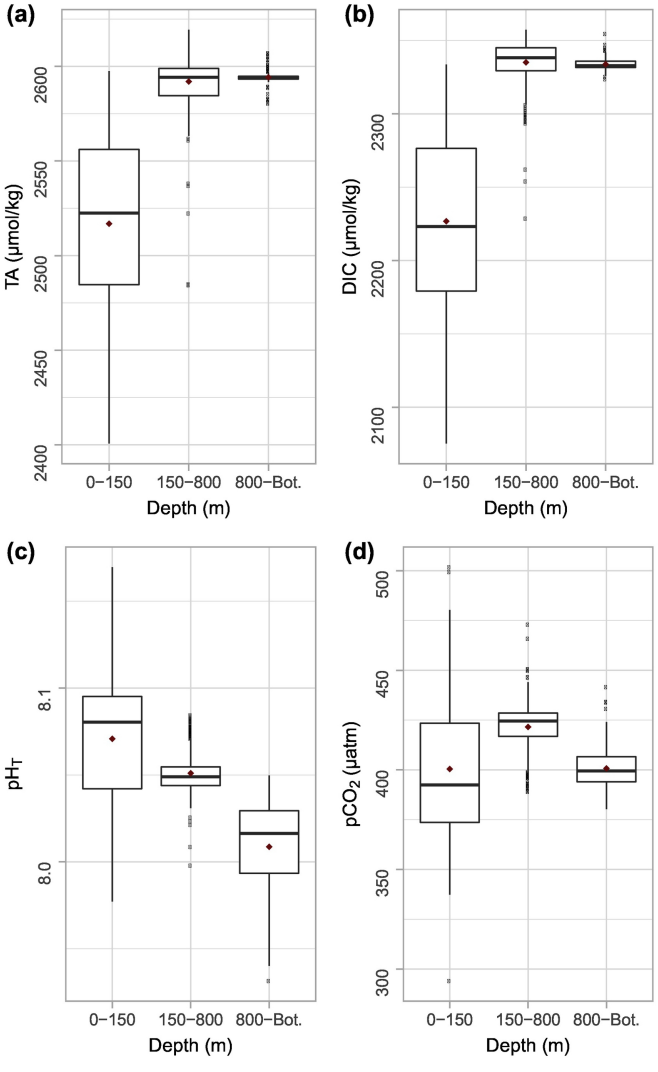
(a)
TA (µmol/kg)
2400
2450
2500
2550
2600
0–150
150–800
800–Bot.
Depth (m)
(b)
DIC (µmol/kg)
2100
2200
2300
0–150
150–800
800–Bot.
Depth (m)
(c)
pH$_T$
8.0
8.1
0–150
150–800
800–Bot.
Depth (m)
(d)
pCO$_2$ (µatm)
300
350
400
450
500
0–150
150–800
800–Bot.
Depth (m)

Figure 4

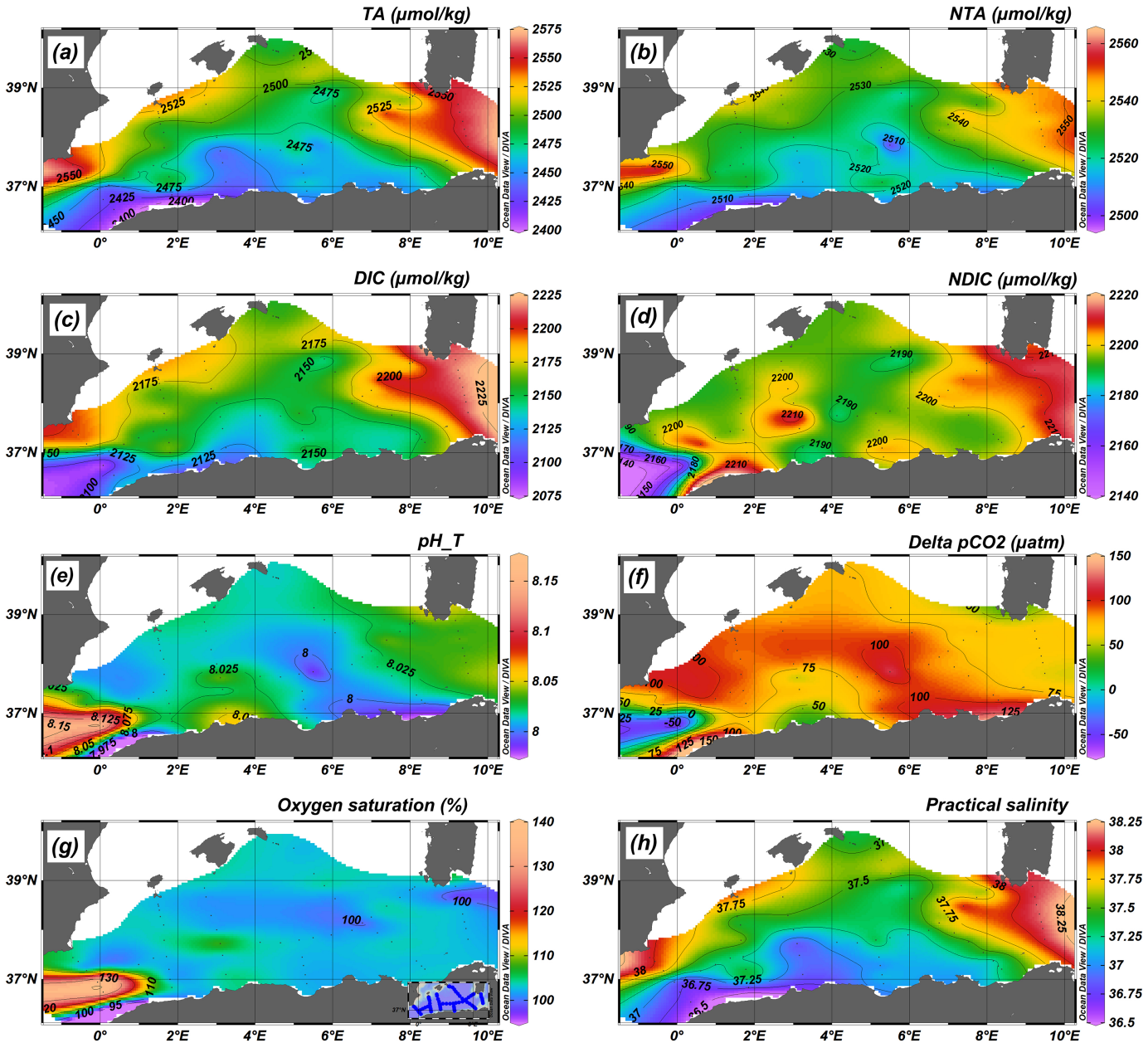
TA (µmol/kg)
(a)
NTA (µmol/kg)
(b)
DIC (µmol/kg)
(c)
NDIC (µmol/kg)
(d)
pH_T
(e)
Delta pCO2 (µatm)
(f)
Oxygen saturation (%)
(g)
Practical salinity
(h)
39°N
37°N
0°
2°E
4°E
6°E
8°E
10°E
Ocean Data View / DIVA

Figure 5

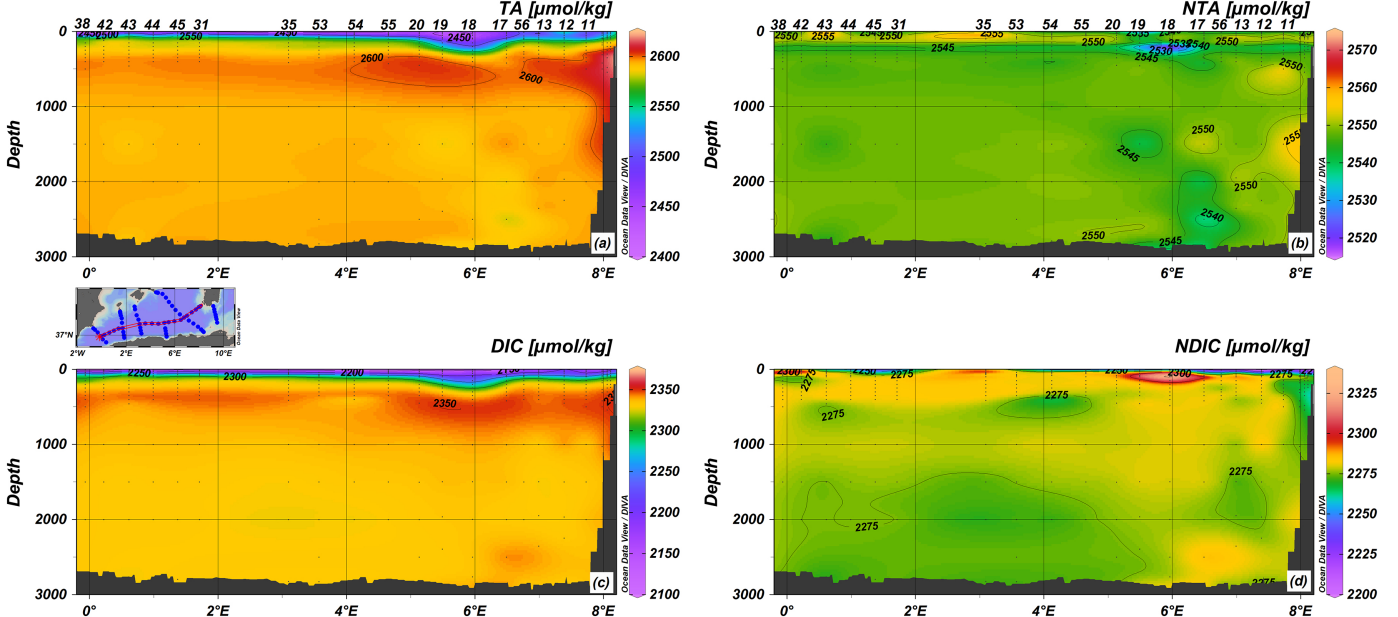
TA [µmol/kg]
NTA [µmol/kg]
DIC [µmol/kg]
NDIC [µmol/kg]
Depth
0
1000
2000
3000
0°
2°E
4°E
6°E
8°E
(a)
(b)
(c)
(d)
37°N
2°W
2°E
6°E
10°E
Ocean Data View / DIVA

Figure 6

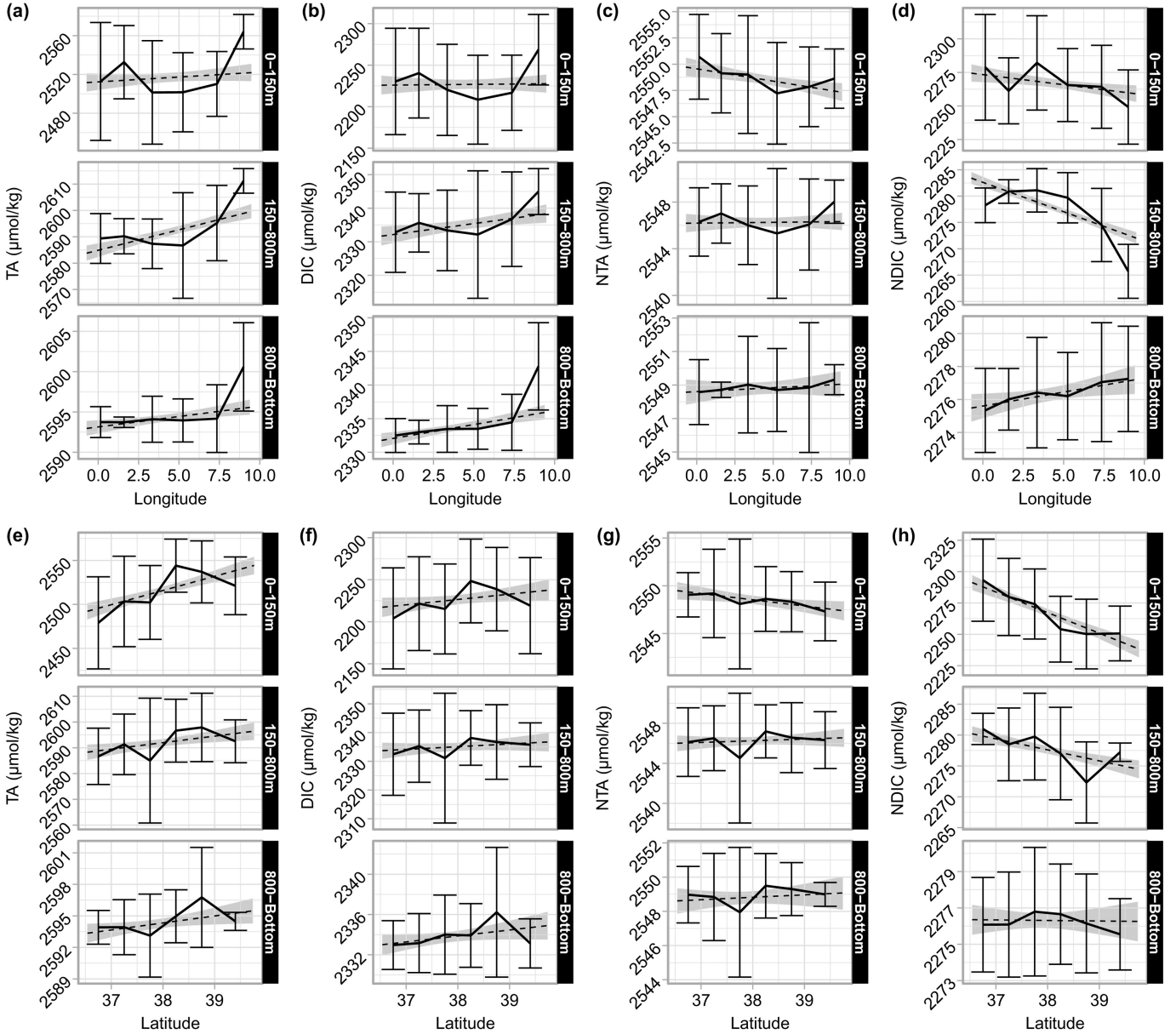
(a)
(b)
(c)
(d)
(e)
(f)
(g)
(h)
0–150m
150–800m
800–Bottom
TA (μmol/kg)
DIC (μmol/kg)
NTA (μmol/kg)
NDIC (μmol/kg)
Longitude
Latitude

Figure 7

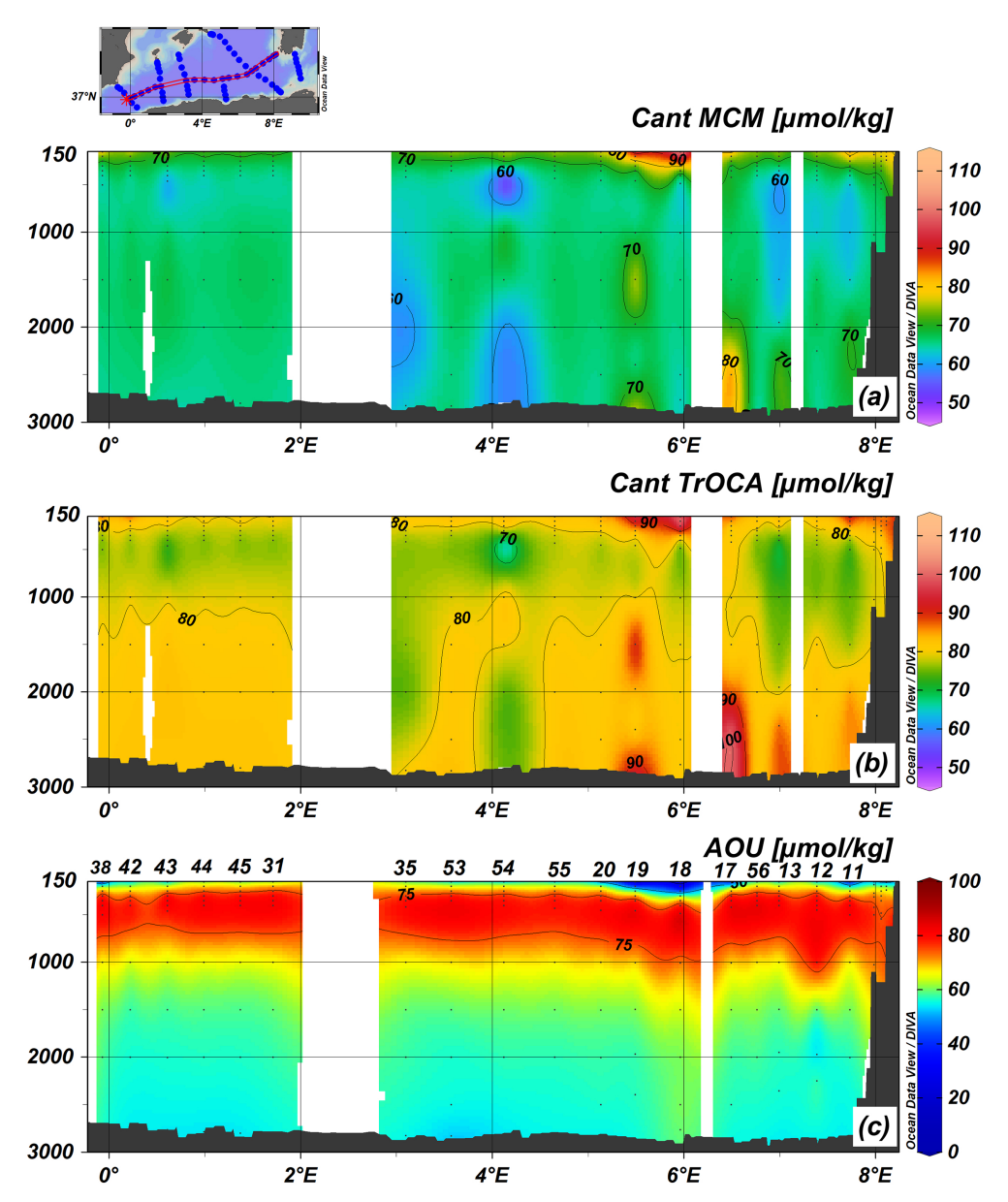
37°N
0°
4°E
8°E
Ocean Data View
Cant MCM [µmol/kg]
(a)
Cant TrOCA [µmol/kg]
(b)
AOU [µmol/kg]
(c)
150
1000
2000
3000
0°
2°E
4°E
6°E
8°E
Ocean Data View / DIVA
110
100
90
80
70
60
50
40
30
20
0

Figure 8

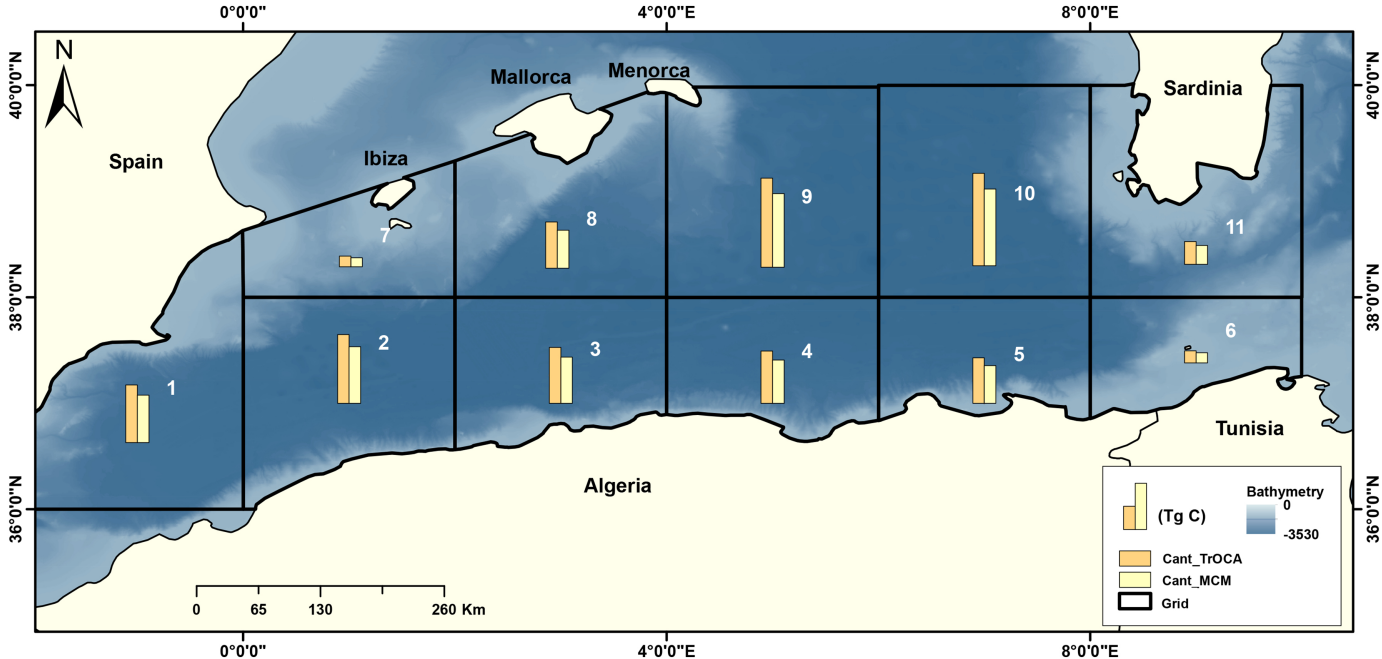
0°0'0"
4°0'0"E
8°0'0"E
40°0'0"N
38°0'0"N
36°0'0"N
N
Spain
Mallorca
Menorca
Ibiza
Sardinia
Algeria
Tunisia
1
2
3
4
5
6
7
8
9
10
11
(Tg C)
Bathymetry
0
-3530
Cant_TrOCA
Cant_MCM
Grid
0
65
130
260 Km

Figure 9

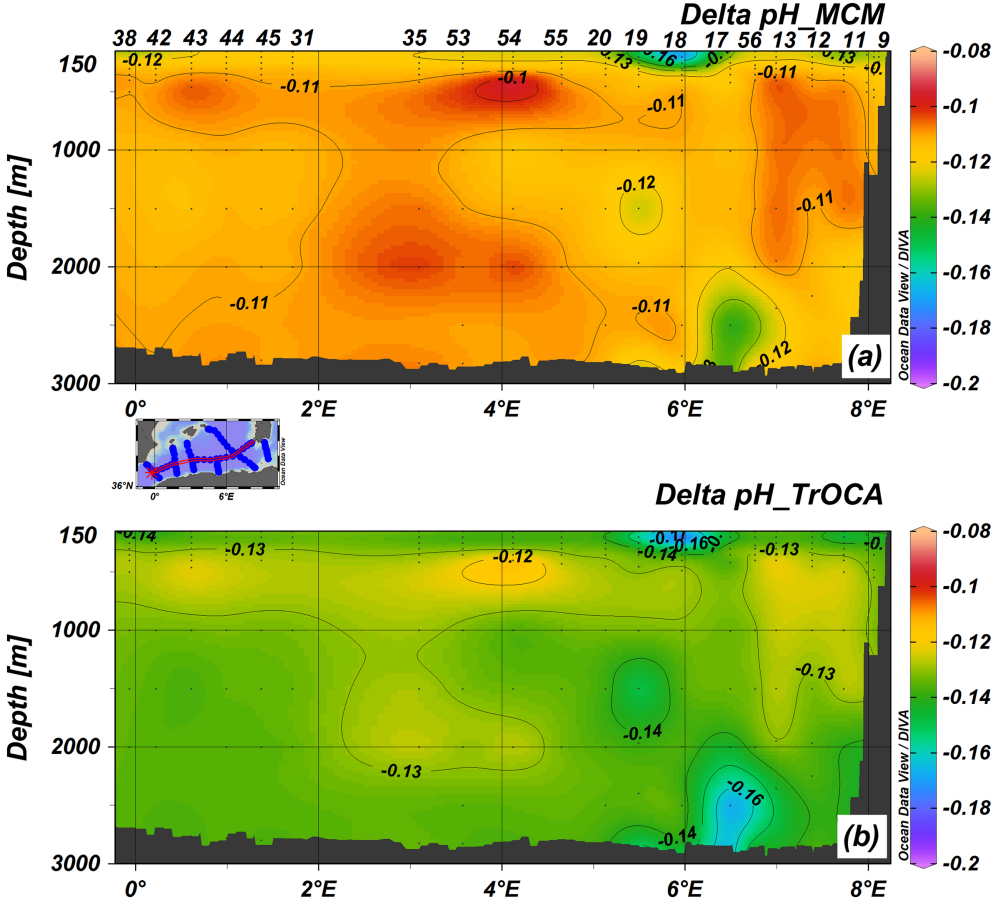
Delta pH_MCM
38 42 43 44 45 31 35 53 54 55 20 19 18 17 56 13 12 11 9
Depth [m]
150
1000
2000
3000
-0.12
-0.11
-0.1
-0.11
-0.12
-0.11
-0.11
-0.11
-0.12
0°
2°E
4°E
6°E
8°E
(a)
-0.08
-0.1
-0.12
-0.14
-0.16
-0.18
-0.2
Ocean Data View / DIVA
36°N
0°
6°E
Ocean Data View
Delta pH_TrOCA
Depth [m]
150
1000
2000
3000
-0.13
-0.12
-0.13
-0.13
-0.14
-0.13
-0.16
-0.14
0°
2°E
4°E
6°E
8°E
(b)
-0.08
-0.1
-0.12
-0.14
-0.16
-0.18
-0.2
Ocean Data View / DIVA

Figure 10